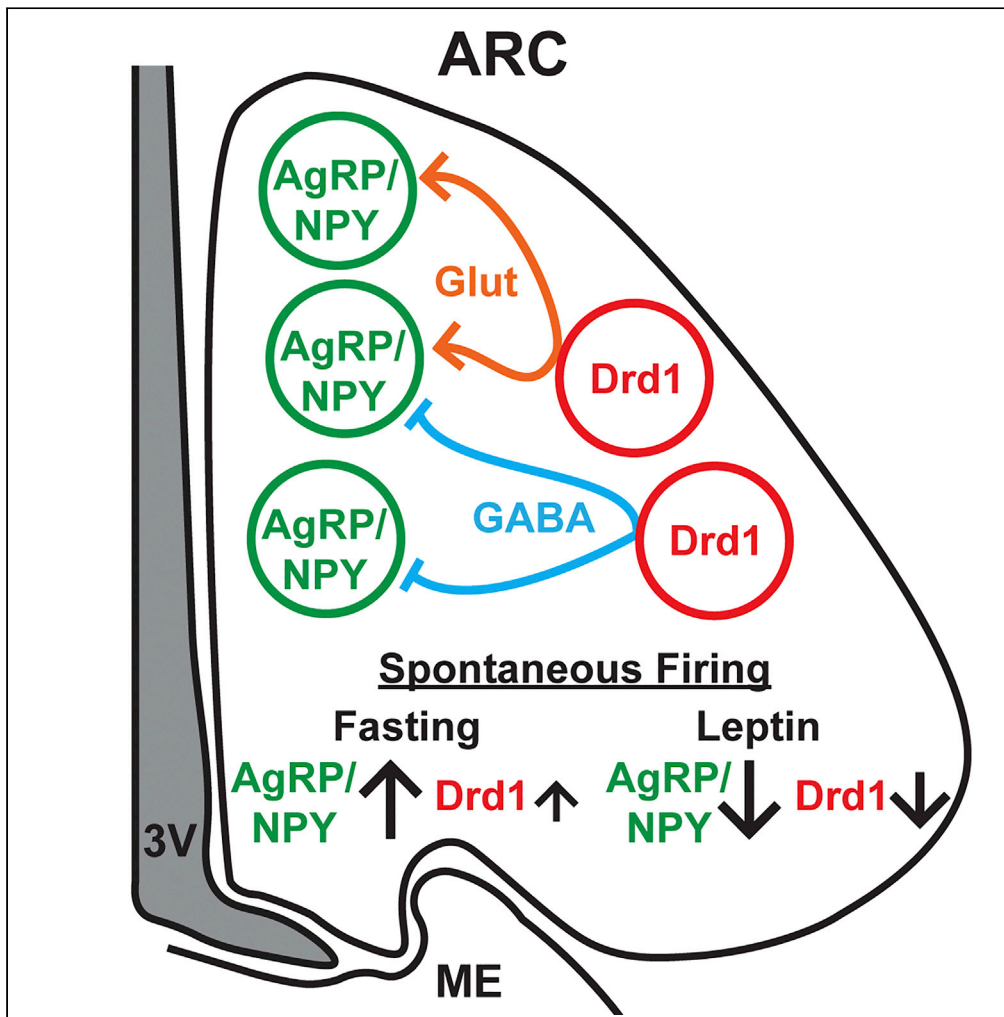


Article

Local Drd1-neurons input to subgroups of arcuate AgRP/NPY-neurons



Sean R. Chadwick,
Ali D. Güler

aguler@virginia.edu

Highlights

ARC^{Drd1+} neurons are less responsive to fasting compared to ARC^{AgRP/NPY+} neurons

ARC^{Drd1+} neurons are inhibited by leptin

ARC^{Drd1+} neurons can either inhibit or excite a subset of ARC^{AgRP/NPY+} neurons

Some ARC^{AgRP/NPY+} neurons receive both GABAergic and glutamatergic ARC^{Drd1+} inputs



Article

Local Drd1-neurons input to subgroups of arcuate AgRP/NPY-neurons

Sean R. Chadwick¹ and Ali D. Güler^{1,2,3,*}

SUMMARY

Obesity is a pandemic afflicting more than 300 million people worldwide, driven by consumption of calorically dense and highly rewarding foods. Dopamine (DA) signaling has been implicated in neural responses to highly palatable nutrients, but the exact mechanisms through which DA modulates homeostatic feeding circuits remains unknown. A subpopulation of arcuate (ARC) agouti-related peptide (AgRP)/neuropeptide Y (NPY) ($ARC^{AgRP/NPY+}$) neurons express the D(1A) dopamine receptor (Drd1) and are stimulated by DA, suggesting one potential avenue for dopaminergic regulation of food intake. Using patch clamp electrophysiology, we evaluated the responses of ARC Drd1-expressing (ARC^{Drd1+}) neurons to overnight fasting and leptin. Collectively, ARC^{Drd1+} neurons were less responsive to caloric deficit than $ARC^{AgRP/NPY+}$ neurons; however, ARC^{Drd1+} neurons were inhibited by the satiety hormone leptin. Using Channelrhodopsin-2-Assisted Circuit Mapping, we identified novel subgroups of ARC^{Drd1+} neurons that inhibit or excite $ARC^{AgRP/NPY+}$ neurons. These findings suggest dopamine receptive neurons have multimodal actions in food intake circuits.

INTRODUCTION

Throughout the world, human diets are increasingly composed of high calorie food, a development that represents a major factor contributing to the obesity pandemic (Kearney, 2010; Statovci et al., 2017). Overeating is the primary driver of obesity, and consumption of fat and sugar activates the brain's innate reward systems (Berridge et al., 2010; Verdejo-Román et al., 2017). Obese individuals suffer from a plethora of comorbid conditions including type 2 diabetes, cardiovascular disease, cancer, and metabolic syndrome (Engin, 2017; Powell-Wiley et al., 2021; Scully et al., 2020; Bhaskaran et al., 2014), and these conditions significantly reduce lifespan and create an enormous burden on healthcare systems (Cawley and Meyerhoefer, 2012). Except for invasive bariatric surgery, current treatments for obesity such as altered diet are inadequate for controlling patient weight, particularly over protracted periods of time (Mann et al., 2007). Elucidation of how reward systems impinge on energy balance circuits is necessary to develop better treatment strategies in the fight against this public health crisis.

Within the CNS, the arcuate nucleus of the hypothalamus (ARC) is an essential integrator of peripheral signals that reflect metabolic states (Cone et al., 2001; Dietrich and Horvath, 2013; Sternson et al., 2013). Landmark experiments demonstrated that activation of ARC agouti-related peptide (AgRP) neurons, which co-express Neuropeptide Y (NPY) (hereinafter referred to as $ARC^{AgRP/NPY+}$ neurons), is sufficient to invoke voracious feeding, even in sated animals (Aponte et al., 2011; Krashes et al., 2011; Atasoy et al., 2012; Betley et al., 2013). $ARC^{AgRP/NPY+}$ neurons are modulated by hormones and neurotransmitters secreted during states of caloric deficit and surplus (Cone et al., 2001; Aponte et al., 2011; Garfield et al., 2016). For instance, $ARC^{AgRP/NPY+}$ neurons increase their firing in response to orexigenic peptides including ghrelin, orexin, neuromedin B, or gastric releasing hormone (GRH) (Hewson et al., 2002; van den Pol et al., 2009; Kohno and Yada, 2012; Mandelblat-Cerf et al., 2015; Cowley et al., 2003; Chen et al., 2017). Conversely, $ARC^{AgRP/NPY+}$ neuron firing is decreased in response to peptide YY, insulin, or leptin (Xu et al., 2005; Takahashi and Cone, 2005; Yang et al., 2010; Bouret et al., 2012; Baver et al., 2014; Jones et al., 2019). $ARC^{AgRP/NPY+}$ neurons release gamma-aminobutyric acid (GABA), AgRP, and NPY onto their downstream targets, and these inhibitory outputs drive different aspects of feeding behaviors (Krashes et al., 2013; Atasoy et al., 2012; Betley et al., 2013). Today, $ARC^{AgRP/NPY+}$ neurons are recognized as a crucial orexigenic population in energy homeostasis, but our understanding of

¹Program in Fundamental Neuroscience and the Department of Biology, University of Virginia, Charlottesville, VA 22904, USA

²Department of Neuroscience, School of Medicine, University of Virginia, Charlottesville, VA 22903, USA

³Lead contact

*Correspondence: aguler@virginia.edu
<https://doi.org/10.1016/j.isci.2022.104605>



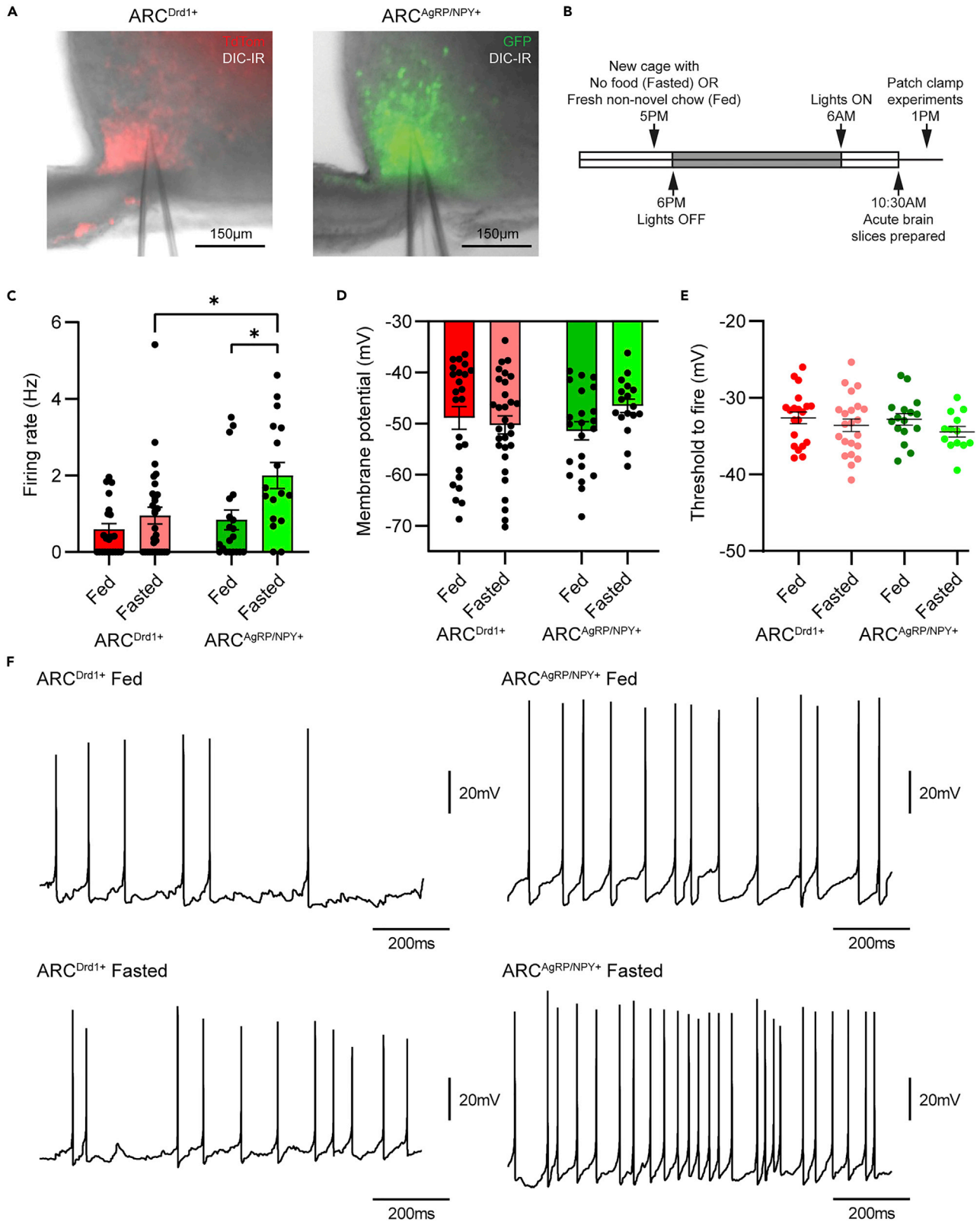


Figure 1. Overnight fasting increases spontaneous firing in ARC^{AgRP/NPY+} neurons but not ARC^{Drd1+} neurons

(A) Representative fluorescence images of ARC^{Drd1+} (TdTom, red) and ARC^{AgRP/NPY+} (GFP, green) neurons. Scale bar 150 μm.

(B) Diagram of overnight fasting experimental setup.

(C) Spontaneous firing rates of ARC^{Drd1+} neurons (n = 24 neurons from fed animals and n = 30 neurons from fasted animals) and ARC^{AgRP/NPY+} neurons (n = 20 neurons from fed animals and 17 neurons from fasted animals). For all groups: (*p < 0.05, **p < 0.01, ***p < 0.001 as determined by two-way ANOVA with Bonferroni post hoc comparison, F_{genotype} (1, 87) = 7.12, p = 0.009; F_{fasting} (1, 87) = 9.73, p = 0.003). Data are represented as mean ± SEM.

(D) Inter spike interval membrane potentials of ARC^{Drd1+} (n = 24 neurons from fed animals and n = 30 neurons from fasted animals) and ARC^{AgRP/NPY+} (n = 20 neurons from fed animals and 17 neurons from fasted animals). For all groups: (*p < 0.05, **p < 0.01, ***p < 0.001 as determined by two-way ANOVA with Bonferroni post hoc comparison, F_{genotype} (1, 87) = 0.104, p = 0.7482; F_{fasting} (1, 87) = 0.830, p = 0.3647).

(E) Firing thresholds of ARC^{Drd1+} (n = 20 neurons from fed animals and 22 neurons from fasted animals) and ARC^{AgRP/NPY+} (n = 16 neurons from fed animals and n = 13 neurons from fasted animals). For all groups: (*p < 0.05, **p < 0.01, ***p < 0.001 as determined by two-way ANOVA with Bonferroni post hoc comparison, F_{genotype} (1, 68) = 0.396 p = 0.531; F_{fasting} (1, 68) = 2.42 p = 0.124).

(F) Representative traces of whole cell current clamp recordings of spontaneous firing. Vertical scale bars, 20 mV. Horizontal scale bars, 200 ms.

the discrete molecular mechanisms governing their activity remains incomplete (Claret et al., 2007; Garfield et al., 2016; Alhadeff et al., 2019; Goldstein et al., 2021).

Current models of food intake circuitry lack explanations for how information about the rewarding properties of food is integrated with homeostatic systems, and researchers have hypothesized that dopamine (DA) may be a key player in hedonic regulation of appetite during the consumption of rewarding and highly palatable foods (Wise, 2006; Palmiter, 2007; Alhadeff et al., 2019; Mazzone et al., 2020). Staining for DA receptors has revealed dopamine one receptor (Drd1) immunoreactivity in the ARC, peri-ARC, and median eminence (ME) (Romero-Fernandez et al., 2014). However, characterization of ARC neuron subtypes has proven challenging (Vong et al., 2011; Krashes et al., 2011; Campbell et al., 2017), and it is unknown which neuronal populations express Drd1 in this region. Recent studies have demonstrated that DA modulates the activity of ARC neurons (Zhang and van den Pol, 2016; Alhadeff et al., 2019), including AgRP neurons that express Drd1 (Zhang and van den Pol, 2016). These results implicate DA signaling as one mechanism through which information about the rewarding properties of drugs and palatable foods integrate into homeostatic circuits.

Using patch clamp electrophysiology, we compared the membrane properties of Drd1-expressing neurons (ARC^{Drd1+}) and ARC^{AgRP/NPY+} neurons. ARC^{Drd1+} neurons exhibited significant inhibitory responses to leptin, although these responses were less drastic than those observed in ARC^{AgRP/NPY+} neurons. Surprisingly, ARC^{Drd1+} neuronal membrane properties were not significantly affected by overnight fasting. To gain better insight into the role of ARC^{Drd1+} neurons in ARC circuitry, we used Channelrhodopsin-2-Assisted Circuit Mapping (CRACM) to identify novel connections from ARC^{Drd1+} neurons to other ARC neurons and characterized these inputs. We established that the ARC^{Drd1+} neuron population is heterogeneous and includes a subpopulation of neurons that co-express AgRP and NPY (ARC^{Drd1+;AgRP/NPY+}). Ultimately, we uncovered subgroups of ARC^{Drd1+} neurons that either inhibit or excite ARC^{AgRP/NPY+} neurons. These findings reveal a complex circuitry where ARC^{Drd1+} neurons can differentially modulate a key population of orexigenic neurons and further our understanding of DA's role in the regulation of appetite.

RESULTS

Overnight fasting increases spontaneous firing in ARC^{AgRP/NPY+} neurons but not ARC^{Drd1+} neurons

wDrd1 expression has been documented in ARC, including in ARC^{AgRP/NPY+} neurons (Romero-Fernandez et al., 2014; Zhang and van den Pol, 2016). However, neurophysiological characteristics of the ARC^{Drd1+} neurons have not been established. Therefore, we determined the electrophysiological properties of ARC^{Drd1+} neurons in comparison to ARC^{AgRP/NPY+} neurons. To visualize Drd1 expressing neurons in the ARC (ARC^{Drd1+}), we crossed Drd1^{tm1(cre)Rpa} (Drd1-Cre) mice (Heusner et al., 2008) with Gt(ROSA)26Sor^{tm14(CAG-tdTomato)Hze} (Ai14 or TdTomato) mice (Madisen et al., 2010), generating Drd1^{cre/+;tdTomato^{td/+}} double transgenic animals, which express TdTomato when Cre recombinase is expressed from the Drd1a locus. In the hypothalamus, we observed tdTomato expression in the ARC, ME, and ventromedial hypothalamus (VMH) (Figures 1A and S1). To visualize ARC^{AgRP/NPY+} neurons, we used Tg(Npy-hrGFP)1Lowl (NPY-GFP) mice (van den Pol et al., 2009), which express GFP under the control of the Npy promoter, labeling NPY neurons in the ARC and other brain regions (Figures 1A and S1). 59.3% ± 3.2% of ARC^{AgRP/NPY+} neurons co-expressed Drd1-TdTom, whereas 52.2% ± 2.9% of ARC^{Drd1+} neurons co-expressed NPY-GFP (from Drd1^{cre/+;tdTomato^{td/+};NPY-GFP^{GFP/+}; triple}

transgenic mice, $n = 3$ animals, four sections per animal) (Figure S1). To establish the baseline electrical behavior of these two neuronal populations, we performed whole cell current clamp and recorded spontaneous firing in fluorescently labeled $\text{ARC}^{\text{Drd1}^+}$ and $\text{ARC}^{\text{AgRP/NPY}^+}$ neurons from animals provided *ad libitum* access to standard chow (henceforth fed $\text{ARC}^{\text{Drd1}^+}$ neurons, and fed $\text{ARC}^{\text{AgRP/NPY}^+}$ neurons, respectively) (Figures 1A–1D). To further assess membrane excitability, a subset of recorded neurons was injected with progressively increasing steps of square current (Figure 1E). Fed $\text{ARC}^{\text{Drd1}^+}$ and $\text{ARC}^{\text{AgRP/NPY}^+}$ neurons did not have significant differences in spontaneous firing rates ($\text{ARC}^{\text{Drd1}^+}$: 0.60 ± 0.15 Hz; $\text{ARC}^{\text{AgRP/NPY}^+}$: 0.84 ± 0.26 Hz; unpaired two-tailed Student's *t*-test $t = 0.846$, $df = 42$, $p = 0.403$), inter spike interval membrane potentials (ISI-MPs) ($\text{ARC}^{\text{Drd1}^+}$: -48.90 ± 2.20 mV; $\text{ARC}^{\text{AgRP/NPY}^+}$: -46.54 ± 1.33 mV; unpaired two-tailed Student's *t*-test $t = 0.720$, $df = 43$, $p = 0.476$), and firing thresholds ($\text{ARC}^{\text{Drd1}^+}$: -32.62 ± 0.77 mV; $\text{ARC}^{\text{AgRP/NPY}^+}$: -32.81 ± 0.75 mV; unpaired two-tailed Student's *t*-test $t = 0.173$, $df = 34$, $p = 0.864$).

$\text{ARC}^{\text{AgRP/NPY}^+}$ neurons become excited during states of caloric deficiency (Takahashi and Cone, 2005; Liu et al., 2012; Wei et al., 2015; Laing et al., 2018), and we hypothesized this phenomenon might also be observable in $\text{ARC}^{\text{Drd1}^+}$ neurons in fasted mice. Therefore, to determine if the electrophysiological properties of $\text{ARC}^{\text{Drd1}^+}$ neurons are impacted by negative energy balance, we fasted $\text{Drd1}^{\text{cre/+}}$; $\text{tdTomato}^{\text{td/+}}$ and NPY-GFP mice overnight and performed whole cell current clamp recordings in fluorescently labeled neurons (Figure 1B). In line with previous reports, $\text{ARC}^{\text{AgRP/NPY}^+}$ neurons from fasted animals (henceforth referred to as fasted $\text{ARC}^{\text{AgRP/NPY}^+}$ neurons) fired at a significantly faster frequency than neurons from fed animals (Figure 1C). Strikingly, the spontaneous firing, ISI-MP and firing threshold of $\text{ARC}^{\text{Drd1}^+}$ neurons from fasted animals (fasted $\text{ARC}^{\text{Drd1}^+}$ neurons) were not significantly different from $\text{ARC}^{\text{Drd1}^+}$ neurons from fed animals (Figures 1C–1E). In addition, fasted $\text{ARC}^{\text{AgRP/NPY}^+}$ neurons fired at a higher frequency than the $\text{ARC}^{\text{Drd1}^+}$ neurons from fasted mice (Figure 1C). Thus, fasting increases the spontaneous firing rate of $\text{ARC}^{\text{AgRP/NPY}^+}$ neurons but not $\text{ARC}^{\text{Drd1}^+}$ neurons, indicating that these neuronal populations may not be identical in terms of their inputs or sensitivity to anorexigenic signals.

$\text{ARC}^{\text{Drd1}^+}$ neurons are inhibited by leptin

$\text{ARC}^{\text{AgRP/NPY}^+}$ neurons are inhibited by sensory cues and peripheral signals of food detection, nutrient consumption, and positive energy equilibrium (Chen et al., 2015; Borgmann et al., 2021; Beutler et al., 2017; Su et al., 2017; Alhadeff et al., 2019; Berrios et al., 2021). One potent inhibitor of $\text{ARC}^{\text{AgRP/NPY}^+}$ neurons is the anorexigenic hormone leptin, which directly hyperpolarizes and silences $\text{ARC}^{\text{AgRP/NPY}^+}$ neurons during states of energy surplus (Takahashi and Cone, 2005; Baver et al., 2014; Bermeo et al., 2020). To ascertain the responses of $\text{ARC}^{\text{Drd1}^+}$ neurons to leptin, we performed whole cell patch clamp electrophysiology on $\text{ARC}^{\text{Drd1}^+}$ and $\text{ARC}^{\text{AgRP/NPY}^+}$ neurons and measured changes in firing rate and membrane potential after a 3 min of perfusion of 100 nM leptin (Figure 2). As expected, bath application of leptin decreased the firing rate of all $\text{ARC}^{\text{AgRP/NPY}^+}$ neurons from fed and fasted animals (Figures 2A–2C). In addition, leptin significantly hyperpolarized all tested fed and fasted $\text{ARC}^{\text{AgRP/NPY}^+}$ neurons (Figure 2D). Although leptin perfusion also inhibited the majority of $\text{ARC}^{\text{Drd1}^+}$ neurons, the hormone's effects were of smaller magnitude compared to responses observed in $\text{ARC}^{\text{AgRP/NPY}^+}$ neurons. In fed $\text{ARC}^{\text{Drd1}^+}$ neurons, bath application of leptin decreased firing rate of all tested neurons (Figures 2E–2G). However, this reduction was only 64% on average, compared to an average 93% reduction in firing rate for fed $\text{ARC}^{\text{AgRP/NPY}^+}$ neurons, a difference that was not statistically significant (unpaired two-tailed Student's *t*-test, $p = 0.13$, $t = 1.64$, $df = 10$, $n = 6$ neurons per group). In addition, although leptin perfusion significantly hyperpolarized fed $\text{ARC}^{\text{Drd1}^+}$ neurons, only 83% of tested neurons had a reduction in membrane potential. Taken with our previous finding that $\text{ARC}^{\text{Drd1}^+}$ neurons had insignificant changes in firing rates because of fasting (Figure 1C), these results indicate heterogeneity in terms of how $\text{ARC}^{\text{Drd1}^+}$ neurons respond to energy balance signals.

$\text{ARC}^{\text{Drd1}^+}$ neurons functionally connect to other ARC neurons

After comparing the effects of fasting and leptin on $\text{ARC}^{\text{Drd1}^+}$ neurons, we evaluated if other ARC neurons receive inputs from $\text{ARC}^{\text{Drd1}^+}$ neurons in the region. To achieve this, we injected an AAV carrying Cre-dependent Channelrhodopsin-mCherry (ChR2-mCh) (Boyden et al., 2005) into the ARC of $\text{Drd1}^{\text{cre/+}}$ mice and performed patch clamp electrophysiology on randomly selected neurons in the ARC (Figure 3). This strategy allowed us to use Channelrhodopsin-2-Assisted Circuit Mapping (CRACM) (Petreanu et al., 2007; Atasoy et al., 2008) to interrogate the postsynaptic responses of ARC neurons following $\text{ARC}^{\text{Drd1}^+}$ neuron activation (Figures 3A–3E). We observed viral expression throughout the basomedial hypothalamus, which is concentrated in the ARC and peri-ARC (Figure 3A).

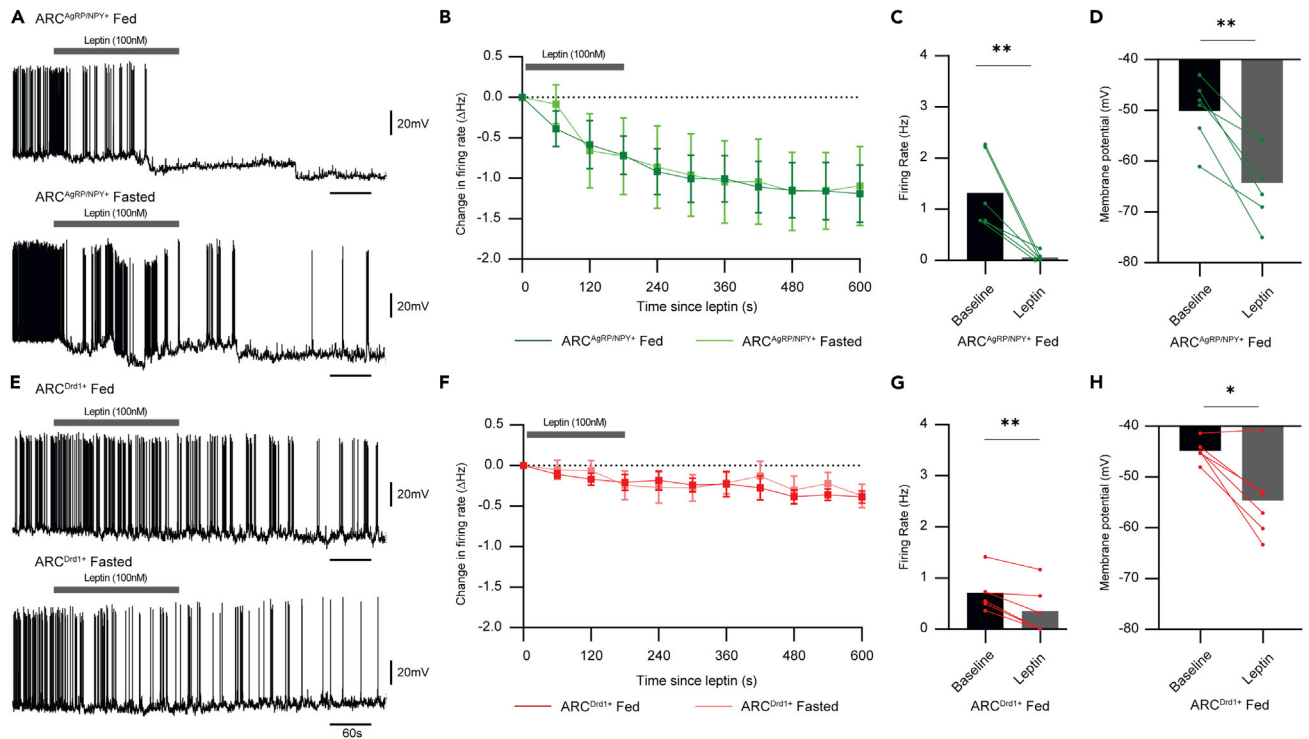


Figure 2. ARC^{Drd1+} neurons are inhibited by leptin

(A) Representative traces of whole cell current clamp recordings of leptin-mediated inhibition in ARC^{AgRP/NPY+} neurons from fed animals (top) and ARC^{AgRP/NPY+} neurons from fasted animals (bottom). Vertical scale bars, 20mV. Horizontal scale bars, 60s.

(B) Change in firing rate from baseline for neurons perfused with leptin, binned for 1-min intervals. Each data point represents the average firing in the previous 60 s. Green: fed ARC^{AgRP/NPY+} neurons (n = 6); light green: fasted ARC^{AgRP/NPY+} neurons (n = 7). Data are represented as mean ± SEM.

(C) Firing rate at baseline and 8 min after the start of leptin perfusion for ARC^{AgRP/NPY+} neurons from fed animals (*p < 0.05, **p < 0.01, ***p < 0.001 as determined by paired two-tailed Student's t-test, t = 4.14, df = 5, n = 6 pairs).

(D) Inter spike interval membrane potential at baseline and 8 min after start of leptin perfusion for ARC^{AgRP/NPY+} neurons from fed animals (*p < 0.05, **p < 0.01, ***p < 0.001 as determined by paired two-tailed Student's t-test, t = 5.73, df = 5, n = 6 pairs).

(E) Representative traces of whole cell current clamp recordings of leptin-mediated inhibition in fed ARC^{Drd1+} neurons (top) and fasted ARC^{Drd1+} neurons (bottom). Vertical scale bars, 20mV. Horizontal scale bars, 60s.

(F) Change in firing rate from baseline for neurons perfused with leptin, binned for 1-min intervals. Each data point represents the average firing in the previous 60 s. Red: fed ARC^{Drd1+} neurons (n = 6); pink: fasted ARC^{Drd1+} neurons (n = 6). Data are represented as mean ± SEM.

(G) Firing rate at baseline and 8 min after the start of leptin perfusion for ARC^{Drd1+} neurons from fed animals (*p < 0.05, **p < 0.01, ***p < 0.001 as determined by paired two-tailed Student's t-test, t = 4.95, df = 5, n = 6 pairs).

(H) Inter spike interval membrane potential at baseline and 8 min after start of leptin perfusion for ARC^{Drd1+} neurons from fed animals (*p < 0.05, **p < 0.01, ***p < 0.001 as determined by two-tailed Student's t-test, t = 3.81, df = 5, n = 6 pairs).

We obtained current clamp recordings from 32 neurons in 19 coronal hypothalamic slices from 12 animals. Of these 32 neurons, we identified six neurons that expressed ChR2 (ChR2+), eight neurons with postsynaptic depolarizations, six neurons with postsynaptic hyperpolarizations, and 12 neurons with no discernible response (Figures 3B and 3C). Light stimulation in ChR2+ neurons resulted in a significant change in peak membrane potential from baseline (Figure 3B) and the latency of the response for these neurons was 0.30 ± 0.04 ms (Figure 3E), consistent with the temporal kinetics of ChR2-based neuron activation (Boyden et al., 2005). Light stimulation did not result in a significant change in peak membrane potential from baseline in nonresponders but was significant for neurons with depolarizing and hyperpolarizing responses (Figure 3C). Latency of the response from onset of the light stimulus for depolarizing and hyperpolarizing neurons was 5.16 ± 0.54 ms and 7.46 ± 1.39 ms, respectively (Figure 3E). Because these neurons often demonstrate spontaneous firing and occasionally show postsynaptic depolarization resulting in action potentials, only traces where the analysis window was free of action potentials were analyzed, likely resulting in underestimation of the strength of depolarizing inputs to these neurons. One hyperpolarizing neuron was observed to have an average response latency of 13.9 ms, suggesting the input may have originated from a neuron with an intermediary connection to an upstream ChR2 expressing neuron. To confirm the

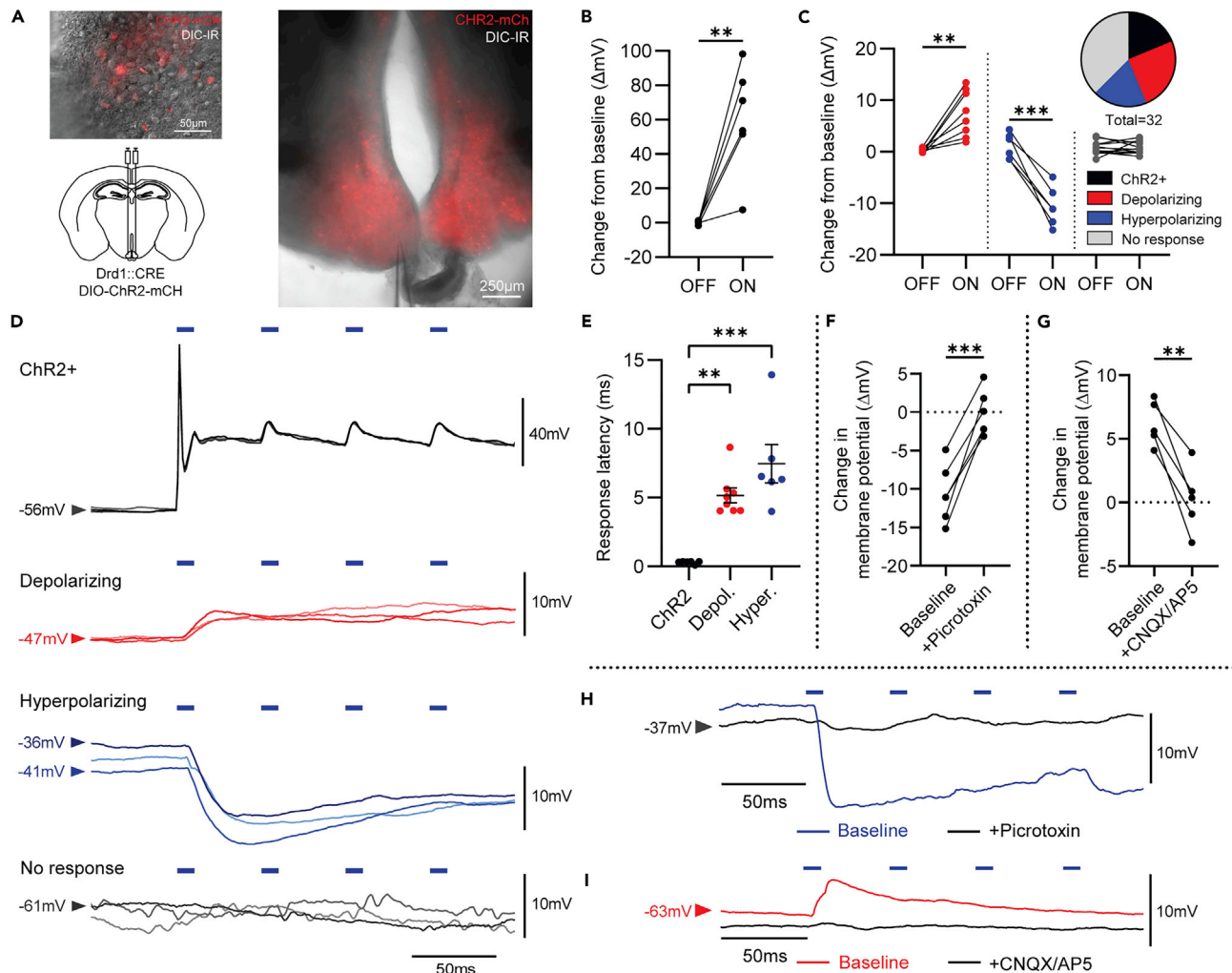


Figure 3. ARC^{Drd1+} neurons functionally connect other ARC neurons

(A) Top left: representative image of 40× DIC IR and fluorescence of ChR2-mCh ARC viral expression in acute coronal brain slices. Bottom left: Schematic of bilateral intracranial injection of Cre dependent ChR2-mCh to the ARC of Drd1-Cre mice. Scale bar 50 μm. Right: representative image of 4× DIC IR and fluorescence of ChR2-mCh ARC viral expression in acute coronal brain slices. Scale bar 250 μm.

(B) Change in membrane potential for light off and on for ChR2 expressing neurons, (*p < 0.05, **p < 0.01, ***p < 0.001 as determined by paired two tailed Student's t-test, t = 4.763, df = 5, n = 6 pairs).

(C) Change in membrane potential of ARC neurons which depolarized, hyperpolarized, or had no response to ARC^{Drd1+} ChR2 inputs. (*p < 0.05, **p < 0.01, ***p < 0.001 as determined by paired two tailed Student's t-test; depolarized: t = 4.763, df = 5, n = 8 pairs; hyperpolarized: t = 3.81, df = 5, n = 6 pairs; no response: t = 3.81, df = 5, n = 12 pairs). Top right: pie chart summary recorded responses in ARC neurons. (*p < 0.05, **p < 0.01, ***p < 0.001 as determined by paired two tailed Student's t-test).

(D) Representative whole cell current clamp traces for responses to four light stimulations, three individual traces from the same neuron shown per response type. For ChR2+, vertical scale bar = 40 mV. For depolarizing, hyperpolarizing, and no response, vertical scale bar = 10 mV. All horizontal scale bars, 50 ms.

(E) Latency from light onset to response initiation for responding neurons. (*p < 0.05, **p < 0.01, ***p < 0.001 as determined by ordinary one-way ANOVA with Bonferroni post hoc comparison, n = 6–8/group; F_{group} = 1.85 (2, 17), p = <0.001). Error bars represent mean ± SEM.

(F) Change in membrane potential for hyperpolarizing neurons during baseline and after 5 min from the start of the perfusion of PTX. (*p < 0.05, **p < 0.01, ***p < 0.001 as determined by paired two-tailed Student's t-test, t = 8.440, df = 5, n = 6 pairs, p = <0.001).

(G) Change in membrane potential for depolarizing neurons during baseline and after 5 min from the start of the perfusion of CNQX/AP5. (*p < 0.05, **p < 0.01, ***p < 0.001 as determined by paired two-tailed Student's t test, t = 6.428, df = 4, n = 5 pairs, p = <0.003).

(H) Representative trace of extinction of hyperpolarization response after 5 min of PTX perfusion. Vertical scale bars, 10 mV. Horizontal scale bars, 50 ms. (I) Representative trace of extinction of depolarization response after 5 min of CNQX/AP5 perfusion. Vertical scale bars, 10 mV. Horizontal scale bars, 50 ms.

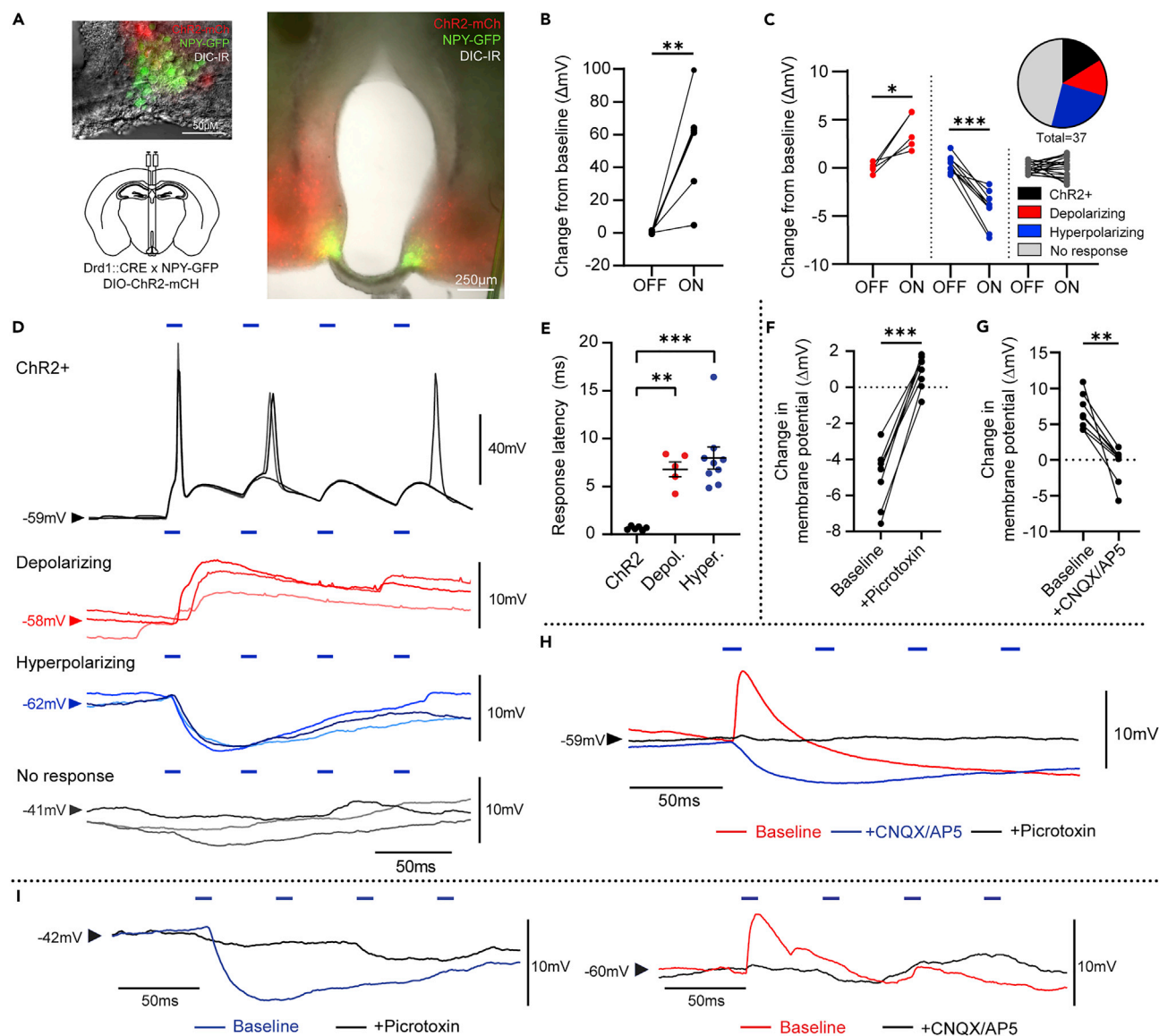


Figure 4. ARC^{Drd1+} neurons make functional connections to $ARC^{AgRP/NPY+}$ neurons, and $ARC^{AgRP/NPY+}$ neurons include a subpopulation of ARC^{Drd1+} neurons

(A) Top left: representative image of 40 \times DIC IR and fluorescence of ChR2-mCh ARC viral expression and ARC NPY-GFP expression in acute coronal brain slices. Scale bar 50 μ m. Bottom left: schematic of bilateral intracranial injection of Cre-dependent ChR2-mCherry (ChR2-mCh) to the ARC of $Drd1^{Cre/+}; NPY^{Gfp/+}$ mice. Right: representative image of 4 \times DIC IR and fluorescence of ChR2-mCh ARC viral expression and ARC NPY-GFP expression in acute coronal brain slices. Scale bar 250 μ m.

(B) Change in membrane potential for light off and on for ChR2 expressing $ARC^{AgRP/NPY+}$ expressing neurons ($*p < 0.05$, $**p < 0.01$, $***p < 0.001$ as determined by paired two tailed Student's *t*-test, $t = 4.038$, $df = 5$, $n = 6$ pairs). Analysis was conducted in an identical manner to those in Figure 3B.

(C) Change in membrane potential of $ARC^{AgRP/NPY+}$ neurons that depolarized, hyperpolarized, or had no response to ARC^{Drd1+} ChR2 inputs. ($*p < 0.05$, $**p < 0.01$, $***p < 0.001$ as determined by paired two tailed Student's *t*-test; depolarized: $t = 4.149$, $df = 4$, $n = 5$ pairs; hyperpolarized: $t = 7.494$, $df = 8$, $n = 9$ pairs); No response: $t = 0.1774$, $df = 16$, $p = 0.861$, $n = 12$ pairs). Top right: pie chart summary for responses recorded in $ARC^{AgRP/NPY+}$ neurons ($*p < 0.05$, $**p < 0.01$, $***p < 0.001$ as determined by paired two tailed Student's *t*-test, $t = 4.149$, $df = 4$, $n = 5$ pairs). Analysis was conducted in an identical manner to those in Figure 3C.

(D) Representative whole cell current clamp traces for various responses to light stimulation, three individual traces from the same $ARC^{AgRP/NPY+}$ neuron shown per response type. For ChR2+, vertical scale bar = 40 mV. For depolarizing, hyperpolarizing, and no response, vertical scale bar = 10 mV. All horizontal scale bars, 50 ms.

(E) Latency from light onset to response initiation for responding $ARC^{AgRP/NPY+}$ neurons. ($*p < 0.05$, $**p < 0.01$, $***p < 0.001$ as determined by ordinary one-way ANOVA with Bonferroni post hoc comparison, $n = 5-9$ /group; $F_{group} = 1.61$ (2, 17), $p = < 0.001$). Analysis was conducted in an identical manner to those in Figure 3E. Error bars represent mean \pm SEM.

Figure 4. Continued

(F) Change in membrane potential for hyperpolarizing $ARC^{AgRP/NPY+}$ neurons during baseline and after 5 min from the start of PTX perfusion. (* $p < 0.05$, ** $p < 0.01$, *** $p < 0.001$ as determined by paired two-tailed Student's *t* test, $t = 14.2$, $df = 7$, $n = 8$ pairs, $p = <0.001$). Analysis was conducted in an identical manner to those in Figure 3F.

(G) Change in membrane potential for depolarizing $ARC^{AgRP/NPY+}$ neurons during baseline and after 5 min from the start of PTX perfusion. (* $p < 0.05$, ** $p < 0.01$, *** $p < 0.001$ as determined by paired two-tailed Student's *t* test, $t = 5.159$, $df = 7$, $n = 8$ pairs, $p = <0.002$). Analysis was conducted in an identical manner to those in Figure 3F.

(H) Representative trace of extinguishment of depolarization response and then hyperpolarization response of $ARC^{AgRP/NPY+}$ neurons during baseline and after 5 min of CNQX/AP5 perfusion, and then subsequent extinguishment of revealed hyperpolarization response following 5 min of CNQX/AP5 and PTX. Vertical scale bars, 10mV. Horizontal scale bars, 50ms.

(I) Representative trace of extinguishment of hyperpolarization response (left) and depolarization response (right) of $ARC^{AgRP/NPY+}$ neurons during baseline and after 5 min of PTX or CNQX/AP5 perfusion, respectively.

observed hyperpolarizing and depolarizing responses were because of inputs secreting gamma aminobutyric acid (GABA) or glutamate, respectively, a subgroup of neurons were tested with by bath perfusion of either 100 μ M of the gamma aminobutyric acid (GABA) receptor blocker picrotoxin (PTX) or 20 μ M cyanquixaline (CNQX) and 50 μ M D-(–)-2-Amino-5-phosphonopentanoic acid (AP5) (Figures 3F–3I). Bath perfusion of PTX resulted in a significant reduction in the hyperpolarizing response in all tested neurons (Figures 3F and 3H). On average, response magnitudes decreased by 10.46 ± 1.23 mV, confirming the hyperpolarizing inputs observed were GABAergic. Bath perfusion of CNQX and AP5 resulted in a significant reduction in the depolarizing responses in all tested neurons (Figures 3H and 3I). On average, response magnitudes decreased by 5.99 ± 0.93 mV, confirming the depolarizing inputs observed were because of glutamatergic inputs.

ARC^{Drd1+} neurons make functional connections to $ARC^{AgRP/NPY+}$ neurons, and $ARC^{AgRP/NPY+}$ neurons include a subpopulation of ARC^{Drd1+} neurons

Given their anatomical location, $ARC^{AgRP/NPY+}$ neurons likely comprised a substantial subgroup of neurons we recorded from during our initial CRACM experiment (Figure 3). Thus, we hypothesized that some ARC^{Drd1+} neurons may have functional inputs to $ARC^{AgRP/NPY+}$ neurons. To investigate this connection, we injected an AAV carrying Cre-dependent ChR2-mCherry into the ARC of $Drd1^{cre/+}; NPY^{Gfp/+}$ mice resulting in green labeled $ARC^{AgRP/NPY+}$ cells and red labeled ARC^{Drd1+} cells. We then performed patch clamp electrophysiology on GFP labeled $ARC^{AgRP/NPY+}$ neurons, allowing us to evaluate the presence of functional inputs (Figure 4). We observed viral expression throughout the basomedial hypothalamus, concentrated in the ARC and peri-ARC (Figure 4A).

We obtained current clamp recordings from 37 $ARC^{AgRP/NPY+}$ neurons in 13 coronal hypothalamic slices from nine mice. Of these ARC^{NPY+} neurons, we identified six ChR2+ neurons, five neurons with postsynaptic depolarizations, nine neurons with postsynaptic hyperpolarizations, and 17 neurons with no discernible response (Figures 4B–4D). ChR2 expression in $ARC^{AgRP/NPY+}$ neurons confirms that a subpopulation of ARC^{Drd1+} neurons is also AgRP/NPY positive in line with previous findings (Zhang and van den Pol, 2016). Based on these findings, we estimate that at least 16% of $ARC^{AgRP/NPY+}$ neurons co-express *Drd1*, and roughly 38% of $ARC^{AgRP/NPY+}$ neurons tested had observable inputs from ARC^{Drd1+} neurons (14% of which were depolarizing and 24% of which were hyperpolarizing). Light stimulation in ChR2+ $ARC^{AgRP/NPY+}$ neurons resulted in a significant change in peak membrane potential from baseline (Figure 4B), and the latency of the response for these neurons was 0.65 ± 0.08 ms (Figure 4E). For $ARC^{AgRP/NPY+}$ neurons which were classified as nonresponding, light stimulation did not result in a significant change in peak membrane potential compared to baseline but was significant for both depolarizing and hyperpolarizing $ARC^{AgRP/NPY+}$ neurons (Figure 4C). Latency of the response from onset of the light stimulus for depolarizing and hyperpolarizing $ARC^{AgRP/NPY+}$ neurons was 6.80 ± 0.77 ms and 7.98 ± 1.15 ms, respectively (Figure 4E). One hyperpolarizing $ARC^{AgRP/NPY+}$ neuron was observed to have an average response latency of 16.42 ms, again suggesting the input may have originated from a neuron with an intermediary connection to an upstream ChR2 expressing neuron. To confirm the observed hyperpolarizing and depolarizing responses were because of inputs secreting gamma aminobutyric acid (GABA) or glutamate, respectively, a subgroup of neurons were tested with by bath perfusion of either 100 μ M of the gamma aminobutyric acid (GABA) receptor blocker picrotoxin (PTX) or 20 μ M cyanquixaline (CNQX) and 50 μ M D-(–)-2-Amino-5-phosphonopentanoic acid (AP5) (Figures 3F–3I). Bath perfusion PTX resulted in a significant reduction in the hyperpolarizing response in all tested $ARC^{AgRP/NPY+}$ neurons (Figures 4F and 4G). On average, response magnitudes decreased by 5.84 ± 0.41 mV, confirming that the hyperpolarizing inputs from ARC^{Drd1+} neurons \rightarrow $ARC^{AgRP/NPY+}$ neurons observed were GABAergic. Bath perfusion of CNQX and AP5 resulted in a significant reduction in the

depolarizing response in all tested $ARC^{AgRP/NPY+}$ neurons (Figures 4F and 4G). On average, response magnitudes decreased by 7.27 ± 1.41 mV, confirming the depolarizing inputs observed were because of glutamatergic inputs. In addition, one $ARC^{AgRP/NPY+}$ neuron had CNQX/AP5 sensitive depolarizing inputs and displayed hyperpolarizing responses following application of glutamate blockers that were subsequently blocked with PTX (Figure 4H), indicating that some $ARC^{AgRP/NPY+}$ neurons can receive both depolarizing and hyperpolarizing inputs from ARC^{Drd1+} neurons.

DISCUSSION

Responses of ARC^{Drd1+} neurons to signals of metabolic deficit and surplus

We have shown that leptin inhibits ARC^{Drd1+} neurons in a comparable manner to responses observed in the $ARC^{AgRP/NPY+}$ neuronal population. Other patch clamp studies have focused on the effects of small molecules on ARC neurons including leptin (Glau et al., 1996; Cowley et al., 2001; van den Top et al., 2004; Vong et al., 2011; Takahashi and Cone, 2005; Hill et al., 2008), ghrelin (Tong et al., 2008; Kohno and Yada, 2012), DA and DA receptor agonists and antagonists (Zhang and van den Pol, 2016; Alhadeff et al., 2019), insulin (Mirshamsi et al., 2004; Kohno and Yada, 2012), and glucose (Kohno and Yada, 2012; Jais et al., 2020). Our results regarding leptin's action on $ARC^{AgRP/NPY+}$ neurons are in line with previous studies demonstrating leptin-based inhibition of this neuron subtype (Takahashi and Cone, 2005; Baver et al., 2014). Similar responses observed in ARC^{Drd1+} neurons may be explained partially by incidental targeting of the $ARC^{Drd1+;AgRP/NPY+}$ neuron population, which was identified during subsequent CRACM experiments. Interestingly, profiling of the spontaneous firing and membrane properties of ARC^{Drd1+} neurons revealed that, as a whole, they are less responsive than $ARC^{AgRP/NPY+}$ neurons to fasting. Others have also measured the electrophysiological properties of ARC neurons given different experimental treatments, including fasting (Liu et al., 2012), exercise (Han et al., 2018), high fat diet (HFD) (Baver et al., 2014; Wei et al., 2015; Jais et al., 2020), and gastric inputs (Alhadeff et al., 2019; Goldstein et al., 2021; Jais et al., 2020). Ultimately, our results suggest the ARC^{Drd1+} neuronal population is heterogeneous.

Connectivity of ARC^{Drd1+} and $ARC^{AgRP/NPY+}$ neurons

Our CRACM experiments revealed overlap of ARC^{Drd1+} neurons with $ARC^{AgRP/NPY+}$ neurons, presenting a potential site of direct regulation by dopaminergic inputs. Interestingly, we identified two subpopulations of ARC^{Drd1+} neurons which had either hyperpolarizing or depolarizing outputs to $ARC^{AgRP/NPY+}$ neurons. We consider it unlikely that $ARC^{Drd1+} \rightarrow ARC^{AgRP/NPY+}$ neuron connections were in fact $AgRP \rightarrow AgRP$ or $POMC \rightarrow AgRP$ connections, given previous findings on the connectivity of ARC neurons. Studies identified functional $AgRP \rightarrow POMC$ connections, but failed to find functional interconnections within $AgRP$ and $POMC$ populations (i.e., $AgRP \rightarrow AgRP$ and $POMC \rightarrow POMC$) (Atasoy et al., 2012). In addition, no evidence of $POMC \rightarrow AgRP$ connectivity has been identified, despite early speculation of feedback loops (Betley et al., 2013). Thus, $ARC^{Drd1+} \rightarrow ARC^{AgRP/NPY+}$ neurons (i.e., ARC^{Drd1+} neurons which putatively do not express $AgRP/NPY$) represent a unique group of neurons with differential inputs to $ARC^{AgRP/NPY+}$ neurons.

DA signaling in the ARC

Our findings instantiate both direct and indirect mechanisms through which ARC^{Drd1+} neuronal populations could modulate the $ARC^{AgRP/NPY+}$ circuit. Our CRACM experiments confirm the existence of an $ARC^{Drd1+;AgRP/NPY+}$ neuronal population, supporting previous findings that $Drd1$ -dependent signaling can drive direct activation of $ARC^{AgRP/NPY+}$ neurons (Zhang & van den Pol, 2016). Synapses containing DA have been localized to the soma of $ARC^{AgRP/NPY+}$ neurons (Zhang & van den Pol, 2016); however, the circumstances that precipitate DA release at these terminals are unknown. Our lab recently found that mice fed an HFD have increased DA tone in other hypothalamic regions containing $Drd1$ expressing neurons (Grippo et al., 2020), and the occurrence of a comparable phenomenon in the ARC remains a distinct possibility. In one potential model, in response to a palatable diet, DA levels in the ARC would increase, stimulating the $Drd1$ expressing $AgRP$ neurons, whereas inhibiting $POMC$ neurons via dopamine receptor 2 ($Drd2$) signaling (Zhang & van den Pol, 2016). Such signaling could drive increased feeding, perhaps even in sated animals, but the dopaminergic inputs or the specific molecular pathways underlying DA receptor signaling in ARC neuron subtypes are unknown.

In addition to the $ARC^{Drd1+;AgRP/NPY+}$ neuronal population, we identified two additional groups of ARC^{Drd1+} neurons which had inhibitory or excitatory inputs to $ARC^{AgRP/NPY+}$ neurons. The circumstances driving activation of various ARC^{Drd1+} subtypes are unknown, and different signals may elicit distinct

ARC^{Drd1+} → ARC^{AgRP/NPY+} inputs. However, evidence supports DA mediated inhibition of ARC^{AgRP/NPY+} neurons in response to gastric signals. In experiments performed by Alhadeff et al., intragastric infusions of nutrients and ethanol increased midbrain DA signaling and inhibited ARC^{AgRP/NPY+} neurons. Infusion of a DA receptor antagonist cocktail was shown to dampen these inhibitory responses during reward delivery (Alhadeff et al., 2019), but the mechanism underlying this DA signaling was not elucidated. These findings are potentially counterintuitive, given the results presented by Zhang et al., who observed that DA and the Drd1 selective agonist SKF 38393 excite AgRP neurons (Zhang & van den Pol, 2016). In addition to a multi-neuronal inhibitory circuit, our work provides another bridge between these results, showing ARC^{Drd1+} neurons can both activate or inhibit ARC^{AgRP/NPY+} neurons. This is supported by the growing body of evidence that DA and Drd1 can have differential actions in the same brain region (Trudeau et al., 2014; Miller et al., 2019). For instance, Miller et al. showed different medial amygdala dopamine one receptor (MeApv-D1R) neurons possess outputs with divergent functional connections, where MeApv-D1R neurons send excitatory outputs to the dorsal medial region of the ventromedial hypothalamus (VMHdm) and inhibitory projections to the bed nucleus of the stria terminalis (BNST) (Miller et al., 2019). Further highlighting the potential complexity of the system, Miller et al. found that the selective Drd1 agonist SKF 81297 increased the excitability of BNST projecting MeApv-D1R neurons, whereas decreasing the excitability of VMH projecting MeApv-D1R neurons. Only with retrograde labeling of MeApv-D1R projections were the investigators ultimately able to distinguish these two subpopulations of Drd1^{cre/+}-tdTomato^{td/+}-labeled neurons in the same nucleus. An analogous phenomenon may be occurring in populations of ARC^{Drd1+} neurons in our study. ARC^{Drd1+} neurons in close proximity may possess differential responses to the same factor, and complete functional characterization of distinct ARC^{Drd1+} subpopulations will require segmentation by inputs, projections, and additional markers.

Limitations of the study

Leptin signaling can have differential effects in different subgroups of ARC neurons. Because this study focused on leptin's inhibitory actions, we cannot rule out the possibility that some ARC^{Drd1+} neurons would have had responses to leptin that are not typically detectable in quiescent or hyperpolarized neurons with membrane potentials below -50mV (Smith et al., 2018). In addition, because of occasional spreading of the viral infusion along the injection needle track, we cannot rule out that some Drd1 inputs may have originated from glutaminergic or GABAergic cells above the ARC, which has previously been documented (Krashes et al., 2014; Suyama and Yada, 2018). Furthermore, this report describes the electrophysiological properties and functional connections of a specific subset of neurons labeled by Drd1-Cre and NPY-GFP; besides, although these transgenic systems have been previously used to corroborate the presence of functional Drd1 and Npy protein or mRNA in labeled neurons (Heusner et al., 2008; van den Pol et al., 2009; Zhang and van den Pol, 2016; Miller et al., 2019), this study did not validate functional signaling in the ARC neurons of these mice. Future studies will evaluate the response of ARC^{Drd1+} neurons to DA and selective agonists to further examine the role ARC Drd1 signaling plays in shaping animal behavior and metabolism.

STAR★METHODS

Detailed methods are provided in the online version of this paper and include the following:

- KEY RESOURCES TABLE
- RESOURCE AVAILABILITY
 - Lead contact
 - Materials availability
 - Data and code availability
- EXPERIMENTAL MODEL AND SUBJECT DETAILS
- METHOD DETAILS
 - Mouse diets
 - Viral expression and stereotaxic surgery
 - Viral constructs
 - Slice electrophysiology
- QUANTIFICATION AND STATISTICAL ANALYSIS
 - Histology, confocal fluorescence microscopy and image processing

SUPPLEMENTAL INFORMATION

Supplemental information can be found online at <https://doi.org/10.1016/j.isci.2022.104605>.

ACKNOWLEDGMENTS

We are especially thankful for technical assistance from Qi Zhang, Qijun Tang, Ryan Grippo, Aundrea Rainwater, and Tarun Vipra. We are also grateful to Ignacio Provencio, Christopher Deppmann, Masashi Kawasaki, Manoj Patel, and Sarah Goggin for their feedback.

This work was supported by NIH National Institute of General Medicinal Sciences R01GM121937, 1R35GM140854 (A.D.G.), UVA Brain Institute 2018 Seed Funding Award (A.D.G.). We acknowledge the Keck Center for Cellular Imaging at UVA for the usage of the Zeiss 780 microscopy system (PI:AP; NIH-OD016446).

AUTHOR CONTRIBUTIONS

S.R.C. conceived, designed, and performed all experiments, with input from A.D.G. S.R.C. wrote the manuscript with input from A.D.G.

DECLARATION OF INTERESTS

The authors declare no competing interests.

Received: November 23, 2021

Revised: May 2, 2022

Accepted: June 8, 2022

Published: July 15, 2022

REFERENCES

- Alhadeff, A.L., Goldstein, N., Park, O., Klima, M.L., Vargas, A., and Betley, J.N. (2019). Natural and drug rewards engage distinct pathways that converge on coordinated hypothalamic and reward circuits. *Neuron* 103, 891–908.e6. <https://doi.org/10.1016/j.neuron.2019.05.050>.
- Aponte, Y., Atasoy, D., and Sternson, S.M. (2011). AGRP neurons are sufficient to orchestrate feeding behavior rapidly and without training. *Nat. Neurosci.* 14, 351–355. <https://doi.org/10.1038/nn.2739>.
- Atasoy, D., Aponte, Y., Su, H.H., and Sternson, S.M. (2008). A FLEX switch targets Channelrhodopsin-2 to multiple cell types for imaging and long-range circuit mapping. *J. Neurosci.* 28, 7025–7030. <https://doi.org/10.1523/JNEUROSCI.1954-08.2008>.
- Atasoy, D., Betley, J.N., Su, H.H., and Sternson, S.M. (2012). Deconstruction of a neural circuit for hunger. *Nature* 488, 172–177. <https://doi.org/10.1038/nature11270>.
- Baver, S.B., Hope, K., Guyot, S., Bjørbaek, C., Kaczorowski, C., and O'Connell, K.M.S. (2014). Leptin modulates the intrinsic excitability of AgRP/NPY neurons in the arcuate nucleus of the hypothalamus. *J. Neurosci.* 34, 5486–5496. <https://doi.org/10.1523/JNEUROSCI.4861-12.2014>.
- Bermeo, K., Castro, H., Arenas, I., and Garcia, D.E. (2020). AMPK mediates regulation of voltage-gated calcium channels by leptin in isolated neurons from arcuate nucleus. *Am. J. Physiol. Endocrinol. Metabol.* 319, E1112–E1120. <https://doi.org/10.1152/ajpendo.00299.2020>.
- Berridge, K.C., Ho, C.-Y., Richard, J.M., and DiFeliceantonio, A.G. (2010). The tempted brain eats: pleasure and desire circuits in obesity and eating disorders. *Brain Res.* 1350, 43–64. <https://doi.org/10.1016/j.brainres.2010.04.003>.
- Berrios, J., Li, C., Madara, J.C., Garfield, A.S., Steger, J.S., Krashes, M.J., and Lowell, B.B. (2021). Food cue regulation of AGRP hunger neurons guides learning. *Nature* 595, 695–700. <https://doi.org/10.1038/s41586-021-03729-3>.
- Betley, J.N., Cao, Z.F.H., Ritola, K.D., and Sternson, S.M. (2013). Parallel, redundant circuit organization for homeostatic control of feeding behavior. *Cell* 155, 1337–1350. <https://doi.org/10.1016/j.cell.2013.11.002>.
- Beutler, L.R., Chen, Y., Ahn, J.S., Lin, Y.-C., Essner, R.A., and Knight, Z.A. (2017). Dynamics of gut-brain communication underlying hunger. *Neuron* 96, 461–475.e5. <https://doi.org/10.1016/j.neuron.2017.09.043>.
- Bhaskaran, K., Douglas, I., Forbes, H., dos-Santos-Silva, I., Leon, D.A., and Smeeth, L. (2014). Body-mass index and risk of 22 specific cancers: a population-based cohort study of 5–24 million UK adults. *Lancet* 384, 755–765. [https://doi.org/10.1016/S0140-6736\(14\)60892-8](https://doi.org/10.1016/S0140-6736(14)60892-8).
- Borgmann, D., Ciglieri, E., Biglari, N., Brandt, C., Cremer, A.L., Backes, H., Tittgemeyer, M., Wunderlich, F.T., Brüning, J.C., and Fenselau, H. (2021). Gut-brain communication by distinct sensory neurons differently controls feeding and glucose metabolism. *Cell Metabol.* 33, 1466–1482.e7. <https://doi.org/10.1016/j.cmet.2021.05.002>.
- Bouret, S.G., Bates, S.H., Chen, S., Myers, M.G., Jr., and Simerly, R.B. (2012). Distinct roles for specific leptin receptor signals in the development of hypothalamic feeding circuits. *J. Neurosci.* 32, 1244–1252. <https://doi.org/10.1523/JNEUROSCI.2277-11.2012>.
- Boyden, E.S., Zhang, F., Bamberg, E., Nagel, G., and Deisseroth, K. (2005). Millisecond-timescale, genetically targeted optical control of neural activity. *Nat. Neurosci.* 8, 1263–1268. <https://doi.org/10.1038/nn1525>.
- Campbell, J.N., Macosko, E.Z., Fenselau, H., Pers, T.H., Lyubetskaya, A., Tenen, D., Goldman, M., Versteegen, A.M.J., Resch, J.M., McCarroll, S.A., et al. (2017). A molecular census of arcuate hypothalamus and median eminence cell types. *Nat. Neurosci.* 20, 484–496. <https://doi.org/10.1038/nn.4495>.
- Cawley, J., and Meyerhoefer, C. (2012). The medical care costs of obesity: an instrumental variables approach. *J. Health Econ.* 31, 219–230. <https://doi.org/10.1016/j.jhealeco.2011.10.003>.
- Chen, S.-R., Chen, H., Zhou, J.-J., Pradhan, G., Sun, Y., Pan, H.-L., and Li, D.-P. (2017). Ghrelin receptors mediate ghrelin-induced excitation of agouti-related protein/neuropeptide Y but not pro-opiomelanocortin neurons. *J. Neurochem.* 142, 512–520. <https://doi.org/10.1111/jnc.14080>.
- Chen, Y., Lin, Y.-C., Kuo, T.-W., and Knight, Z.A. (2015). Sensory detection of food rapidly modulates arcuate feeding circuits. *Cell* 160, 829–841. <https://doi.org/10.1016/j.cell.2015.01.033>.

- Claret, M., Smith, M.A., Batterham, R.L., Selman, C., Choudhury, A.I., Fryer, L.G.D., Clements, M., Al-Qassab, H., Heffron, H., Xu, A.W., et al. (2007). AMPK is essential for energy homeostasis regulation and glucose sensing by POMC and AgRP neurons. *J. Clin. Investig.* *117*, 2325–2336. <https://doi.org/10.1172/JCI31516>.
- Cone, R.D., Cowley, M.A., Butler, A.A., Fan, W., Marks, D.L., and Low, M.J. (2001). The arcuate nucleus as a conduit for diverse signals relevant to energy homeostasis. *Int. J. Obes. Relat. Metab. Disord.* *25* (Suppl 5), S63–S67. <https://doi.org/10.1038/sj.ijo.0801913>.
- Cowley, M.A., Smart, J.L., Rubinstein, M., Cerdán, M.G., Diano, S., Horvath, T.L., Cone, R.D., and Low, M.J. (2001). Leptin activates anorexigenic POMC neurons through a neural network in the arcuate nucleus. *Nature* *411*, 480–484. <https://doi.org/10.1038/35078085>.
- Cowley, M.A., Smith, R.G., Diano, S., Tschöp, M., Pronchuk, N., Grove, K.L., Strasburger, C.J., Bidlingmaier, M., Esterman, M., Heiman, M.L., et al. (2003). The distribution and mechanism of action of ghrelin in the CNS demonstrates a novel hypothalamic circuit regulating energy homeostasis. *Neuron* *37*, 649–661. [https://doi.org/10.1016/s0896-6273\(03\)00063-1](https://doi.org/10.1016/s0896-6273(03)00063-1).
- Dietrich, M.O., and Horvath, T.L. (2013). Hypothalamic control of energy balance: insights into the role of synaptic plasticity. *Trends Neurosci.* *36*, 65–73. <https://doi.org/10.1016/j.tins.2012.12.005>.
- Engin, A. (2017). The definition and prevalence of obesity and metabolic syndrome. In *Obesity and Lipotoxicity*, A.B. Engin and A. Engin, eds. (Springer International Publishing), pp. 1–17. https://doi.org/10.1007/978-3-319-48382-5_1.
- Garfield, A.S., Shah, B.P., Burgess, C.R., Li, M.M., Li, C., Steger, J.S., Madara, J.C., Campbell, J.N., Kroeger, D., Scammell, T.E., et al. (2016). Dynamic GABAergic afferent modulation of AgRP neurons. *Nat. Neurosci.* *19*, 1628–1635. <https://doi.org/10.1038/nn.4392>.
- Glaum, S.R., Hara, M., Bindokas, V.P., Lee, C.C., Polonsky, K.S., Bell, G.I., and Miller, R.J. (1996). Leptin, the obese gene product, rapidly modulates synaptic transmission in the hypothalamus. *Mol. Pharmacol.* *50*, 230–235. <https://www.ncbi.nlm.nih.gov/pubmed/8700128>.
- Goldstein, N., McKnight, A.D., Carty, J.R.E., Arnold, M., Betley, J.N., and Alhadeff, A.L. (2021). Hypothalamic detection of macronutrients via multiple gut-brain pathways. *Cell Metabol.* *33*, 676–687.e5. <https://doi.org/10.1016/j.cmet.2020.12.018>.
- Grippo, R.M., Tang, Q., Zhang, Q., Chadwick, S.R., Gao, Y., Altherr, E.B., Sipe, L., Purohit, A.M., Purohit, N.M., Sunkara, M.D., et al. (2020). Dopamine signaling in the suprachiasmatic nucleus enables weight gain associated with hedonic feeding. *Curr. Biol.* *30*, 196–208.e8. <https://doi.org/10.1016/j.cub.2019.11.029>.
- Han, Y., Xia, G., and Wu, Q. (2018). Functional interrogation of the AgRP neural circuits in control of appetite, body weight, and behaviors. In *Neural Regulation of Metabolism*, Q. Wu and R. Zheng, eds. (Springer Singapore), pp. 1–16. https://doi.org/10.1007/978-981-13-1286-1_1.
- Heusner, C.L., Beutler, L.R., Houser, C.R., and Palmiter, R.D. (2008). Deletion of GAD67 in dopamine receptor-1 expressing cells causes specific motor deficits. *Genesis* *46*, 357–367. <https://doi.org/10.1002/dvg.20405>.
- Hewson, A.K., Tung, L.Y.C., Connell, D.W., Tookman, L., and Dickson, S.L. (2002). The rat arcuate nucleus integrates peripheral signals provided by leptin, insulin, and a ghrelin mimetic. *Diabetes* *51*, 3412–3419. <https://doi.org/10.2337/diabetes.51.12.3412>.
- Hill, J.W., Williams, K.W., Ye, C., Luo, J., Balthasar, N., Coppari, R., Cowley, M.A., Cantley, L.C., Lowell, B.B., and Elmquist, J.K. (2008). Acute effects of leptin require PI3K signaling in hypothalamic proopiomelanocortin neurons in mice. *J. Clin. Investig.* *118*, 1796–1805. <https://doi.org/10.1172/JCI32964>.
- Jais, A., Paeger, L., Sotelo-Hitschfeld, T., Bremser, S., Prinzensteiner, M., Klemm, P., Mykytiuk, V., Widdershooven, P.J.M., Vesting, A.J., Grzelka, K., et al. (2020). PNOCARC neurons promote hyperphagia and obesity upon high-fat diet feeding. *Neuron* *106*, 1009–1025.e10. <https://doi.org/10.1016/j.neuron.2020.03.022>.
- Jones, E.S., Nunn, N., Chambers, A.P., Østergaard, S., Wulff, B.S., and Luckman, S.M. (2019). Modified peptide YY molecule attenuates the activity of NPY/AgRP neurons and reduces food intake in male mice. *Endocrinology* *160*, 2737–2747. <https://doi.org/10.1210/en.2019-00100>.
- Kearney, J. (2010). Food consumption trends and drivers. *Philos. Trans. R. Soc. Lond. Ser. B Biol. Sci.* *365*, 2793–2807. <https://doi.org/10.1098/rstb.2010.0149>.
- Kohno, D., and Yada, T. (2012). Arcuate NPY neurons sense and integrate peripheral metabolic signals to control feeding. *Neuropeptides* *46* (6), 315–319. <https://doi.org/10.1016/j.npep.2012.09.004>.
- Krashes, M.J., Koda, S., Ye, C., Rogan, S.C., Adams, A.C., Cusher, D.S., Maratos-Flier, E., Roth, B.L., and Lowell, B.B. (2011). Rapid, reversible activation of AgRP neurons drives feeding behavior in mice. *J. Clin. Investig.* *121*, 1424–1428. <https://doi.org/10.1172/JCI46229>.
- Krashes, M.J., Shah, B.P., Koda, S., and Lowell, B.B. (2013). Rapid versus delayed stimulation of feeding by the endogenously released AgRP neuron mediators GABA, NPY, and AgRP. *Cell Metabol.* *18*, 588–595. <https://doi.org/10.1016/j.cmet.2013.09.009>.
- Krashes, M.J., Shah, B.P., Madara, J.C., Olson, D.P., Strohlic, D.E., Garfield, A.S., and Lowell, B.B. (2014). An excitatory paraventricular nucleus to AgRP neuron circuit that drives hunger. *Nature* *507* (7491), 238–242. <https://doi.org/10.1038/nature12956>.
- Laing, B.T., Li, P., Schmidt, C.A., Bunner, W., Yuan, Y., Landry, T., Prete, A., McClung, J.M., and Huang, H. (2018). AgRP/NPY neuron excitability is modulated by metabotropic glutamate receptor 1 during fasting. *Front. Cell. Neurosci.* *12*, 276. <https://doi.org/10.3389/fncel.2018.00276>.
- Liu, T., Kong, D., Shah, B.P., Ye, C., Koda, S., Saunders, A., Ding, J.B., Yang, Z., Sabatini, B.L., and Lowell, B.B. (2012). Fasting activation of AgRP neurons requires NMDA receptors and involves spinogenesis and increased excitatory tone. *Neuron* *73*, 511–522. <https://doi.org/10.1016/j.neuron.2011.11.027>.
- Madisen, L., Zwingman, T.A., Sunkin, S.M., Oh, S.W., Zariwala, H.A., Gu, H., Ng, L.L., Palmiter, R.D., Hawrylycz, M.J., Jones, A.R., et al. (2010). A robust and high-throughput Cre reporting and characterization system for the whole mouse brain. *Nat. Neurosci.* *13*, 133–140. <https://doi.org/10.1038/nn.2467>.
- Mandelblat-Cerf, Y., Ramesh, R.N., Burgess, C.R., Patella, P., Yang, Z., Lowell, B.B., and Andermann, M.L. (2015). Arcuate hypothalamic AgRP and putative POMC neurons show opposite changes in spiking across multiple timescales. *Elife* *4*. <https://doi.org/10.7554/eLife.07122>.
- Mann, T., Tomiyama, A.J., Westling, E., Lew, A.-M., Samuels, B., and Chatman, J. (2007). Medicare’s search for effective obesity treatments: diets are not the answer. *Am. Psychol.* *62*, 220–233. <https://doi.org/10.1037/0003-066X.62.3.220>.
- Mazzone, C.M., Liang-Guallpa, J., Li, C., Wolcott, N.S., Boone, M.H., Southern, M., Kobzar, N.P., Salgado, I.d.A., Reddy, D.M., Sun, F., et al. (2020). High-fat food biases hypothalamic and mesolimbic expression of consummatory drives. *Nat. Neurosci.* *23*, 1253–1266. <https://doi.org/10.1038/s41593-020-0684-9>.
- Miller, S.M., Marcotulli, D., Shen, A., and Zweifel, L.S. (2019). Divergent medial amygdala projections regulate approach-avoidance conflict behavior. *Nat. Neurosci.* *22*, 565–575. <https://doi.org/10.1038/s41593-019-0337-z>.
- Mirshamsi, S., Laidlaw, H.A., Ning, K., Anderson, E., Burgess, L.A., Gray, A., Sutherland, C., and Ashford, M.L.J. (2004). Leptin and insulin stimulation of signalling pathways in arcuate nucleus neurons: PI3K dependent actin reorganization and KATP channel activation. *BMC Neurosci.* *5*, 54. <https://doi.org/10.1186/1471-2202-5-54>.
- Noe, M. (2021). Firing threshold value from an action potential phase plot. *Mathworks Central Answers*. <https://www.mathworks.com/matlabcentral/answers/733193-how-do-i-extract-the-firing-threshold-value-from-an-action-potential-phase-plot>.
- Palmiter, R.D. (2007). Is dopamine a physiologically relevant mediator of feeding behavior? *Trends Neurosci.* *30*, 375–381. <https://doi.org/10.1016/j.tins.2007.06.004>.
- Petreaanu, L., Huber, D., Sobczyk, A., and Svoboda, K. (2007). Channelrhodopsin-2-assisted circuit mapping of long-range callosal projections. *Nat. Neurosci.* *10*, 663–668. <https://doi.org/10.1038/nn1891>.
- Powell-Wiley, T.M., Poirier, P., Burke, L.E., Després, J.P., Gordon-Larsen, P., Lavie, C.J., Lear, S.A., Ndumele, C.E., Neeland, I.J., Sanders, P., and St-Onge, M.-P. (2021). Obesity and cardiovascular disease: a scientific statement from the American heart association. *Circulation* *143*, e984–e1010. <https://doi.org/10.1161/CIR.0000000000000973>.
- Romero-Fernandez, W., Borroto-Escuela, D.O., Vargas-Barroso, V., Narváez, M., Di Palma, M.,

- Agnati, L.F., Larriva Sahd, J., and Fuxe, K. (2014). Dopamine D1 and D2 receptor immunoreactivities in the arcuate-median eminence complex and their link to the tubero-infundibular dopamine neurons. *Eur. J. Histochem.* 58, 2400. <https://doi.org/10.4081/ejh.2014.2400>.
- Schindelin, J., Arganda-Carreras, I., Frise, E., Kaynig, V., Longair, M., Pietzsch, T., Preibisch, S., Rueden, C., Saalfeld, S., Schmid, B., et al. (2012). Fiji: an open-source platform for biological-image analysis. *Nat. Methods* 9, 676–682. <https://doi.org/10.1038/nmeth.2019>.
- Scully, T., Ettela, A., LeRoith, D., and Gallagher, E.J. (2020). Obesity, type 2 diabetes, and cancer risk. *Front. Oncol.* 10, 615375. <https://doi.org/10.3389/fonc.2020.615375>.
- Smith, M.A., Katsouri, L., Virtue, S., Choudhury, A.I., Vidal-Puig, A., Ashford, M.L.J., and Withers, D.J. (2018). Calcium channel CaV2.3 subunits regulate hepatic glucose production by modulating leptin-induced excitation of arcuate pro-opiomelanocortin neurons. *Cell Rep.* 25, 278–287.e4. <https://doi.org/10.1016/j.celrep.2018.09.024>.
- Statovci, D., Aguilera, M., MacSharry, J., and Melgar, S. (2017). The impact of western diet and nutrients on the microbiota and immune response at mucosal interfaces. *Front. Immunol.* 8, 838. <https://doi.org/10.3389/fimmu.2017.00838>.
- Sternson, S.M., Nicholas Betley, J., and Cao, Z.F.H. (2013). Neural circuits and motivational processes for hunger. *Curr. Opin. Neurobiol.* 23, 353–360. <https://doi.org/10.1016/j.conb.2013.04.006>.
- Su, Z., Alhadeff, A.L., and Betley, J.N. (2017). Nutritive, post-ingestive signals are the primary regulators of AgRP neuron activity. *Cell Rep.* 21, 2724–2736. <https://doi.org/10.1016/j.celrep.2017.11.036>.
- Suyama, S., and Yada, T. (2018). New insight into GABAergic neurons in the hypothalamic feeding regulation. *J. Physiol. Sci.* 68, 717–722.
- Takahashi, K.A., and Cone, R.D. (2005). Fasting induces a large, leptin-dependent increase in the intrinsic action potential frequency of orexigenic arcuate nucleus neuropeptide Y/Agouti-related protein neurons. *Endocrinology* 146, 1043–1047. <https://doi.org/10.1210/en.2004-1397>.
- Ting, J.T., Daigle, T.L., Chen, Q., and Feng, G. (2014). Acute brain slice methods for adult and aging animals: application of targeted patch clamp analysis and optogenetics. In *Patch-Clamp Methods and Protocols*, M. Martina and S. Taverna, eds. (Springer), pp. 221–242. https://doi.org/10.1007/978-1-4939-1096-0_14.
- Ting, J.T., Lee, B.R., Chong, P., Soler-Llavina, G., Cobbs, C., Koch, C., Zeng, H., and Lein, E. (2018). Preparation of acute brain slices using an optimized N-Methyl-D-glucamine protective recovery method. *JoVE* 132, 53825. <https://doi.org/10.3791/53825>.
- Tong, Q., Ye, C.-P., Jones, J.E., Elmquist, J.K., and Lowell, B.B. (2008). Synaptic release of GABA by AgRP neurons is required for normal regulation of energy balance. *Nat. Neurosci.* 11, 998–1000. <https://doi.org/10.1038/nn.2167>.
- Trudeau, L.-E., Hnasko, T.S., Wallén-Mackenzie, Å., Morales, M., Rayport, S., and Sulzer, D. (2014). The multilingual nature of dopamine neurons. *Prog. Brain Res.* 211, 141–164. <https://doi.org/10.1016/B978-0-444-63425-2.00006-4>.
- van den Pol, A.N., Yao, Y., Fu, L.-Y., Foo, K., Huang, H., Coppari, R., Lowell, B.B., and Broberger, C. (2009). Neuromedin B and gastrin-releasing peptide excite arcuate nucleus neuropeptide Y neurons in a novel transgenic mouse expressing strong Renilla green fluorescent protein in NPY neurons. *J. Neurosci.* 29, 4622–4639. <https://doi.org/10.1523/JNEUROSCI.3249-08.2009>.
- van den Top, M., Lee, K., Whyment, A.D., Blanks, A.M., and Spanswick, D. (2004). Orexigen-sensitive NPY/AgRP pacemaker neurons in the hypothalamic arcuate nucleus. *Nat. Neurosci.* 7, 493–494. <https://doi.org/10.1038/nn1226>.
- Verdejo-Román, J., Vilar-López, R., Navas, J.F., Soriano-Mas, C., and Verdejo-García, A. (2017). Brain reward system's alterations in response to food and monetary stimuli in overweight and obese individuals. *Hum. Brain Mapp.* 38, 666–677. <https://doi.org/10.1002/hbm.23407>.
- Vong, L., Ye, C., Yang, Z., Choi, B., Chua, S., Jr., and Lowell, B.B. (2011). Leptin action on GABAergic neurons prevents obesity and reduces inhibitory tone to POMC neurons. *Neuron* 71, 142–154. <https://doi.org/10.1016/j.neuron.2011.05.028>.
- Wei, W., Pham, K., Gammons, J.W., Sutherland, D., Liu, Y., Smith, A., Kaczorowski, C.C., and O'Connell, K.M. (2015). Diet composition, not calorie intake, rapidly alters intrinsic excitability of hypothalamic AgRP/NPY neurons in mice. *Sci. Rep.* 5, 16810. <https://doi.org/10.1038/srep16810>.
- Whitt, J.P., Montgomery, J.R., and Meredith, A.L. (2016). BK channel inactivation gates daytime excitability in the circadian clock. *Nat. Commun.* 7, 10837. <https://doi.org/10.1038/ncomms10837>.
- Wise, R.A. (2006). Role of brain dopamine in food reward and reinforcement. *Philos. Trans. R. Soc. Lond. Ser. B Biol. Sci.* 361, 1149–1158. <https://doi.org/10.1098/rstb.2006.1854>.
- Xu, A.W., Kaelin, C.B., Takeda, K., Akira, S., Schwartz, M.W., and Barsh, G.S. (2005). PI3K integrates the action of insulin and leptin on hypothalamic neurons. *J. Clin. Investig.* 115, 951–958. <https://doi.org/10.1172/JCI24301>.
- Yang, M.-J., Wang, F., Wang, J.-H., Wu, W.-N., Hu, Z.-L., Cheng, J., Yu, D.-F., Long, L.-H., Fu, H., Xie, N., and Chen, J.-G. (2010). PI3K integrates the effects of insulin and leptin on large-conductance Ca²⁺-activated K⁺ channels in neuropeptide Y neurons of the hypothalamic arcuate nucleus. *Am. J. Physiol. Endocrinol. Metabol.* 298, E193–E201. <https://doi.org/10.1152/ajpendo.00155.2009>.
- Zhang, X., and van den Pol, A.N. (2016). Hypothalamic arcuate nucleus tyrosine hydroxylase neurons play orexigenic role in energy homeostasis. *Nat. Neurosci.* 19, 1341–1347. <https://doi.org/10.1038/nn.4372>.

STAR★METHODS

KEY RESOURCES TABLE

REAGENT or RESOURCE	SOURCE	IDENTIFIER
Bacterial and virus strains		
rAAV2/EF1a-DIO-hChR2(H134R)-mcherry (Karl Deisseroth)	UNC Chapel Hill Vector Core (Dr. R Jude Samulski)	rAAV2/EF1a-DIO-hChR2(H134R)-mcherry/Lot AV4379J
Chemicals, peptides, and recombinant proteins		
D-(+)-Glucose	SIGMAALDRICH	Cat# D9434
N-D-Methyl-Gluconate	SIGMAALDRICH	Cat# M2004
Potassium Chloride	SIGMAALDRICH	Cat# 9333
Sodium phosphate monobasic	SIGMAALDRICH	Cat# RDD007
Magnesium chloride	SIGMAALDRICH	Cat# M8266
Sodium chloride	SIGMAALDRICH	Cat# 746398
Magnesium sulfate heptahydrate	SIGMAALDRICH	Cat# 63138
HEPES	SIGMAALDRICH	Cat# RDD0022
Dimethyl sulfoxide	GE Healthcare Life Sciences	Cat# D2650
Potassium gluconate	SIGMAALDRICH	Cat# P1847
Sodium bicarbonate	SIGMAALDRICH	Cat# 792519
Sodium hydroxide	SIGMAALDRICH	Cat# 795429
Potassium hydroxide	SIGMAALDRICH	Cat# S5881
Murine leptin	Purotech	Cat# 450-31/Lot#: 012,176
CNQX	TOCRIS/R&D systems Inc.	Cat# 0190/Lot#: 334A/224958
D-AP-V	TOCRIS/R&D systems Inc.	Cat# 0106/Lot# 73A/225991
Picrotoxin	Abcam	Cat# ab120315/Lot#: APN19069-1-1
Critical commercial assays		
RNA extraction kit (RNeasy Lipid Tissue Mini Kit)	QIAGEN	Cat# 74804
reverse transcription kit (SuperScript IV First-Strand Synthesis System)	ThermoFisher	Cat# 18091050
Experimental models: Organisms/strains		
Mouse: Drd1-Cre; Drd1aCre/+	Palmiter Lab, University of Washington	N/A
Mouse: NPY-GFP	The Jackson Laboratory	B ₆ .FVB-Tg(Npy-hrGFP)1Low/J Stock No: 006417 NPY-hrGFP , NPY-GFP
C57Bl6/J	The Jackson Laboratory	JAX stock #000664 (https://www.jax.org/strain/000664)
Ai14 TdTomato(Tdt/tdt)	The Jackson Laboratory	JAX stock #007909 (https://www.jax.org/strain/007909)
Oligonucleotides		
Primer: NPY-GFP Common Forward TAT GTG GAC GGG GCA GAA GAT CCA GG	Integrated DNA Technologies	JAX oIMR6223
Primer: NPY-GFP Wild type Reverse CCC AGC TCA CAT ATT TAT CTA GAG	Integrated DNA Technologies	JAX oIMR6224
Primer: NPY-GFP Mutant Reverse GGT GCG GTT GCC GTA CTG GA	Integrated DNA Technologies	JAX oIMR6225

(Continued on next page)

Continued

REAGENT or RESOURCE	SOURCE	IDENTIFIER
Primer: Drd1a::CRE Common Forward TTC TGG TAT GGC TTG GAT TG	Integrated DNA Technologies	N/A
Primer: Drd1a::CRE Wild type Reverse GTG AGG ATG CGA AAG GAG AA	Integrated DNA Technologies	N/A
Primer: Drd1a::CRE Mutant Reverse GGG AAA CCA TTT CCG GTT ATT C	Integrated DNA Technologies	N/A
Primer: Ai14 TdTom Wild type Forward AAG GGA GCT GCA GTG GAG TA	Integrated DNA Technologies	JAX oIMR9020
Primer: Ai14 TdTom Wild type Reverse CCG AAA ATC TGT GGG AAG TC	Integrated DNA Technologies	JAX oIMR9021
Primer: Ai14 TdTom Mutant Reverse GGC ATT AAA GCA GCG TAT CC	Integrated DNA Technologies	JAX oIMR9103
Primer: Ai14 TdTom Mutant Forward CTG TTC CTG TAC GGC ATG G	Integrated DNA Technologies	JAX oIMR9105

Software and algorithms

MATLAB R2020a	MathWorks	https://www.mathworks.com/products/matlab.html
Prism 9	GraphPad Software	https://www.graphpad.com/scientific-software/prism/
QImaging Ocular Software	Photometrics	https://www.scientifica.uk.com/products/qimaging-ocular-software
ImageJ	NIH	https://imagej.nih.gov/ij/RRID:SCR_003070
Clampex Suite with ClampFit 11	Molecular Devices	https://www.moleculardevices.com/products/axon-patch-clamp-system/acquisition-and-analysis-software/pclamp-software-suite
LinLab micromanipulator control software	Scientifica	https://www.scientifica.uk.com/products/scientifica-linlab-2
iPython (with Python v3.8.13)	iPython development team	https://ipython.org/

Other

Stereotaxic apparatus	David Kopf Instruments	Model:1900
Standard chow diet (Teklad F6 Rodent Diet)	Envigo	8664 (production is terminated)
Standard chow diet (PicoLab Rodent Diet 20 5053)	LabDiet	Cat# 0007688
Compresstome Tissue Slicer	Precisionary	Model: VF-200 with manual micrometer
Single Sample Osmometer	Advanced Instruments	Model: 3D3
ThermoFisher HM 505 EVP	ThermoFisher	Model: HM 505 EVP
Signal amplifier	Axon Instruments	Multiclamp 700B
Signal digitizer	Axon Instruments	Axon Digidata 1550B
Fluorescent LED light source	CoolLED	pE-300
4 valve solenoid perfusion exchange system, with hardware controller and 4 channel manifold	Automate Scientific	Economy Valve Pinch System
Patch electrode headstage	Molecular Devices	1-CV7-B
Isoflurane	Primal Critical Care/Covetrus	NDC 11695-6777-2
Ketamine HCl (Ketaset)	Zoetis	NDC 54771-2013-1
ENDURIUM Injector Solid Ceramic blades	Cadance	Cat#: EF-INZ10
Bupivacaine-HCl (Sensoricaine-MPF)	Fresenius Kabi	Cat# NDC63323-464-02
Xylazine (AnaSed Injection)	Akorn Inc.	NDC59399-111-50
DAPI Fluoromount-G	Southern Biotech	Cat# OB010020

RESOURCE AVAILABILITY

Lead contact

Further information and requests should be directed to and will be fulfilled by the Lead Contact, Ali D. Güler (aguler@virginia.edu).

Materials availability

This study did not generate new unique reagents or mouse lines.

Data and code availability

All data and any additional information required to reanalyze the data reported is available from the [Lead contact](#) upon request.

EXPERIMENTAL MODEL AND SUBJECT DETAILS

All animal experiments were conducted in compliance with the University of Virginia Institutional Animal Care and Use Committee (IACUC). Animals were provided cotton nesting material (Ancare, Bellmore, NY) and animal cages were individually ventilated and temperature and humidity controlled, (approx. 40% humidity, 22-24°C). Animals were housed on a 12 hour light/dark cycle, and given water and food *ad libitum*, except for approved periods of time during fasting experiments. The following mouse lines were used: *Drd1*^{tm1(cre)Rpa} (Heusner et al., 2008), *Gt(ROSA)26Sor*^{tm14(CAG-tdTomato)Hze}, (Madisen et al., 2010), *Tg(Npy-hrGFP)1Lowl* (van den Pol et al., 2009). *Drd1*^(Cre/Cre) (KO) mice and littermates bred for husbandry were raised on standard chow diet PicoLab Rodent Diet 20 5053 (LabDiet, USA) placed on the cage floor to facilitate access to the food for the *Drd1*-KO mice. For surgery and confocal imaging experiments, male and female mice were sacrificed for sample preparation when they were between 14 and 21 weeks old. For all other experiments, including fasting and leptin experiments, male and female mice ages P31 to P58 were used.

METHOD DETAILS

Mouse diets

Standard chow diet (SCD): PicoLab Rodent Diet 20 5053 (3.07 kcal/gram; 13% fat, 24% protein, 62% carbohydrates; 3.2% sucrose).

Viral expression and stereotaxic surgery

All surgery was performed on male and female mice between 8 and 14 weeks of age using aseptic technique in compliance with the University of Virginia IACUC. Surgical anesthesia was induced with 5% isoflurane (Isothesia) and then maintained at 2% to 2.5% throughout the procedure. After induction animals were mounted in a stereotaxic frame (Kopf) with an electric heating pad underneath to maintain body temperature. Veterinary ocular lubricant was used on each animal's eyes and reapplied as necessary to prevent dehydration/desiccation. A recombinant AAV was used to express a specific transgene, containing a double-floxed inverted open reading frame (DIO cassette). Virus was delivered at 100 nL/min by a microsyringe pump controller (World Precision Instruments, model Micro 4), via a 10 µL syringe (Hamilton) and 26-gauge needle (Hamilton). After infusion of the AAV was completed, the syringe was left in place for 10 min, after which it was retracted 0.2 mm and then left in place for another 10 minutes before being withdrawn completely. As an analgesic, for 24 hours before and for three days after surgery mice were provided with 30 mg/kg ibuprofen drinking solution (4.7 mL Children's Motrin dissolved in 500 mL sterile water). Mice were then sacrificed for optogenetic experiments 6 to 11 weeks after intracranial injections.

Viral constructs

rAAV2/EF1a-DIO-hChR2(H134R)-mCherry (300nL; diluted to $\sim 1.2 \times 10^{12}$ viral genomes/ul with sterile PBS) was injected into the ARC (ML: ± 0.29 mm, AP: -0.30 mm, DV: -5.75 mm). All coordinates are relative to bregma (George Paxinos and Keith B. J. Franklin). AAV2 version of in stock vector AAV-EF1a-DIO-hChR2(H134R)-mCherry vector (Karl Deisseroth) was purchased from UNC Chapel Hill Virus Vector Core Dr. R Jude Samulski.

Slice electrophysiology

Acute brain slice preparation methods including Na⁺ spike protocol were adapted from (Ting et al., 2014, 2018). When preparing acute brain slices from surgery animals, mice were IP injected with a mixture of ketamine/xylazine and transcardially perfused with roughly 30mL of ice cold NMDG-ACSF containing in mM: 93 NMDG; 2.5 KCl, 1.2 NaH₂PO₄, 30 NaHCO₃, 20 HEPES, and 25 dextrose, 5 sodium ascorbate, 2 thiourea, 3 sodium pyruvate, 10 MgSO₄·7H₂O, 0.5 CaCl₂·2H₂O, saturated with 95% O₂ and 5% CO₂. The brain was then rapidly dissected and 300μm sections containing the hypothalamus were taken using a Compressome VF-200 in ice-cold NMDG-ACSF. Slices were incubated in 34°C NMDG-ACSF and after completion of the Na⁺ spike protocol (Ting et al., 2018) the slices were transferred to a high HEPES low Ca²⁺ buffer holding buffer at 34°C and allowed to come to room temperature where they were held until transfer to microscope for recording. HEPES buffer contained in mM: 92 NaCl, 2.5 KCl, 1.2 NaH₂PO₄, 30 NaHCO₃, 20 HEPES, and 25 dextrose, 5 sodium ascorbate, 2 thiourea, 3 sodium pyruvate, 10 MgSO₄·7H₂O, 0.5 CaCl₂·2H₂O, saturated with 95% O₂ and 5% CO₂. Mice lacking ChR2 expression or which had mistargeting of the viral infusion, were not included in this study. For non-surgery animals, male and female mice ages P31 to P58 were decapitated after being deeply anesthetized with isoflurane using the jar drop method. Brains were rapidly dissected and mounted for slicing in the compressome slicer. Slices were taken in an ice cold sucrose cutting solution containing (in mM): 200 sucrose, 26 NaHCO₃, 1.25 Na₂HPO₄, 3.5 KCl, 10 glucose, 3.8 MgCl₂, 1.2 MgSO₄, pH was adjusted to 7.3 to 7.4 and osmolarity ranged from 299 to 302 mOsm (Whitt et al., 2016). Slices were then transferred to the same high HEPES low Ca²⁺ holding buffer described above at 34°C and allowed to come to room temperature where they were held until transfer to microscope for recording. In all experiments slices were allowed to rest for a minimum of 45 minutes before transfer to a Slicescope 6000 microscope with 4× dry and 40× water immersion Nikon objectives. For all whole cell current clamp recordings, the bath was superfused with a continuous flow (2.5 mL/min) of recording aCSF at room temperature (26°C–28°C), containing the following (in mM): 119 NaCl, 2.5 KCl, 1.25 NaH₂PO₄, 24 NaHCO₃, 12.5 glucose, 2 mM CaCl₂·4H₂O and 2 mM MgSO₄·7H₂O, saturated with 95% O₂ and 5% CO₂ (Ting et al., 2018). For all extracellular solutions, osmolarity ranged from 299 to 302 mOsm and pH was adjusted with strong HCl and ranged from 7.3 to 7.4. Coronal slices containing the ARC were identified visually by the shape of the both 3rd ventricle and the presence of medial eminence. To target ARC^{AgRP/NPY+} neurons for patching, NPY-GFP fluorescence was excited and visualized using a pE-300-white LED light source and GFP filter set. Images of patched brain regions were taken using Scientifica camera and Ocular imaging software. A Multiclamp 700B amplifier and Digidata 1550B digitizer (Molecular Devices) were used to perform all patch clamp experiments. Voltage measurements were digitized at 50 kHz and bridge balance was monitored closely. All experiments were conducted using 3–6MΩ microelectrodes pulled with a Sutter P97 puller. For all current clamp recordings, the pipette was backfilled with an intracellular solution adapted from (Miller et al., 2019) containing, in mM: 135 K-gluconate, 10 HEPES, 3.5 NaCl, 1 EGTA, 5 Mg-ATP, 0.5 Na₃-GTP. For intracellular solution, osmolarity ranged from 290 to 295 and pH was adjusted with KOH and ranged from 7.3 to 7.4. For each neuron, recordings measuring spontaneous firing rate were taken each lasting a minimum of 90 seconds. No holding current was used during whole cell recordings of spontaneous firing. Offline the recordings were analyzed using a combination of ClampFit (Molecular devices) and custom scripts in Matlab (Mathworks) software. Statistical tests were performed in Prism 9 (Graphpad). Light stimulation consisted of 10ms square pulses of light delivered at 20Hz (10 pulses total). Light stimulation was delivered by the high (40×) magnification objective to a hexagonal area approximately 250 μm diameter centered on the recorded cell, and the same light intensity was maintained for all recordings. To report changes in membrane potential and latency in CRACM experiments, 3 to 6 traces (typically 5 or 6 traces) were analyzed. Non-responding cells were confirmed to be healthy by either observation of normal spontaneous firing or minor current injection to elicit action potentials. For each trace the absolute peak value reached relative to baseline was identified within the 50ms immediately after stimulus onset. Results were then averaged for all traces analyzed for that recording. Some neurons spontaneously fired action potentials during the pre or post stimulus analysis window, and traces where this occurred were excluded from analysis, and only cases where the analysis window fell within an inter spike interval were included. For all experiments involving drug perfusions, recordings were acquired only in slices previously treated with pure ACSF. After drug perfusion and washout, no more recordings were made and that slice was discarded. For leptin experiments, only cells with spontaneous firing were chosen for testing. For CNQX/AP5 experiments, a small holding current (<10pA) was used to hold the cell at approximately 60mV. Firing threshold was calculated using scripts adapted from code made available by Mathieu Noe on the Mathworks website (Noe, 2021).

QUANTIFICATION AND STATISTICAL ANALYSIS

When comparing two groups of normally distributed data, a Student's two tailed t test was used. To compare the effects of genotype and fasting within 4 groups, two-way ANOVA test was used. When data was collected from the same animals across time, a three-way ANOVA test was performed to analyze time, genotype and fasting effect. In experiments with a single variable and more than two groups, a one-way ANOVA was performed. Following a significant effect in the ANOVA test, Bonferroni's post hoc comparison was used to determine differences between individual data points. Analyses were conducted using the GraphPad Prism 9 statistical software for Windows. All data are presented as means \pm standard error of the mean with $p < 0.05$ considered statistically significant.

Histology, confocal fluorescence microscopy and image processing

$Drd1^{cre/+};Tdtom^{tdTom/+};NPY^{Gfp/+}$ mice were IP injected with a mixture of ketamine/xylazine and transcardially perfused with roughly 50mL of ice cold 0.01 M phosphate buffer solution (PBS) followed by 50mL ice cold freshly prepared 4% paraformaldehyde (PFA) in PBS, pH 7.3–7.4. Brains were immediately dissected and post-fixed overnight (approximately 20 hours) at 4°C in PFA. Fixed brains were then washed thoroughly in PBS and transferred into a solution of 30% sucrose in PBS for 36 hours, and then embedded in cryostat embedding media in tissue cups and frozen by submerging in a beaker containing isopentyl and dry ice, and stored at -80°C until sectioning. Brains were then sectioned using a cryostat microtome (ThermoFisher HM 505 EVP) and 30 μm coronal sections of the arcuate were collected and transferred to PBS. Sections were then mounted with DAPI Fluoromount-G (Southern Biotech). Images were then collected using a Zeiss LSM780 laser scanning confocal microscope. For post processing confocal microscopy images, no brightness or contrast adjustments were made. To quantify the percentage of AgRP or $Drd1$ -Cre neurons co-expressing TdTom or GFP, 10 \times confocal images taken of sections chosen randomly from consecutive wells, each containing 5 serially collected sections to achieve consistent rostral caudal spacing. Individual neurons were labeled manually using the ImageJ multipoint tool, and a simple Python script was used to identify marked GFP and TdTom neurons within a 5 μm radius of each other. Each label was then subsequently verified manually to ensure accurate co-labeling, in the context of DAPI expression and surrounding marked cells for each channel and group. Arcuate ROI was determined using a combination of Allen Brain Atlas (both Adult reference atlas and ISH coronal images for NPY mRNA expression (experiment 717), NPY-GFP fluorescence in the images, and cell density delineating the blood brain barrier boundary visible through DAPI staining. Finally the ImageJ ROI manager was used to include only neurons marked inside the ROI of the arcuate for analysis. For images shown that were collected during patch clamp experiments using Scientifica camera, the minimum brightness of fluorescent channels (i.e. TdTom or ChR2-mCh, NPY-GFP) was slightly increased to remove out of focus background light using FIJI/ImageJ (Schindelin et al., 2012).